

1
2
3
4
5
6
7
8
9
10
11
12
13
14
15
16
17
18
19
20
21
22
23
24
25
26
27
28
29
30
31
32
33

**The Impacts of Biomass Burning Activities on Convective Systems in
the Maritime Continent**

Hsiang-He Lee^{1*@} and Chien Wang^{1,2**}

¹ Center for Environmental Sensing and Modeling, Singapore-MIT Alliance for Research
and Technology, Singapore

² Center for Global Change Science, Massachusetts Institute of Technology, Cambridge,
MA, U.S.A.

*Now at Atmospheric, Earth, and Energy Division, Lawrence Livermore National
Laboratory, Livermore, CA, U.S.A.

**Now at Laboratoire d'Aerologie/CNRS/University of Toulouse, Toulouse, France

Submitted to
Atmospheric, Chemistry and Physics

July 2019

@Corresponding author address: Dr. Hsiang-He Lee, 7000 East Avenue, Livermore, CA,
94550, U.S.A.

E-mail: lee1061@llnl.gov

34 **Abstract**

35 Convective precipitation associated with Sumatra squall lines and diurnal rainfall
36 over Borneo is an important weather feature of the Maritime Continent in Southeast Asia.
37 Over the past few decades, biomass burning activities have been widespread during
38 summertime over this region, producing massive fire aerosols. These additional aerosols
39 brought to the atmosphere, besides influencing local radiation budget through directly
40 scattering and absorbing sunlight, can also act as cloud condensation nuclei or ice nuclei
41 to alter convective clouds and precipitation in the Maritime Continent via the so-called
42 aerosol indirect effects. Based on four-month simulations with or without biomass
43 burning aerosols conducted using the Weather Research and Forecasting model with
44 chemistry package (WRF-Chem), we have investigated the aerosol-cloud interactions
45 associated with the biomass burning aerosols in the Maritime Continent. Results from
46 selected cases of convective events have shown significant impacts of fire aerosols
47 specifically on the weak convections by increasing the quantities of hydrometeors and
48 rainfall in both Sumatra and Borneo regions. Statistical analysis over the fire season also
49 suggests that fire aerosols have impacts on the nocturnal convections associated with the
50 local anticyclonic circulation in the western Borneo and then weakened the nocturnal
51 rainfall intensity by about 9%. Such an effect is likely come from the near surface
52 heating by absorbing aerosols emitted from fires that could weaken land breezes and thus
53 the convergence of anticyclonic circulation.

54

55

56 **1 Introduction**

57 Biomass burning in Southeast Asia has become a serious environmental and societal
58 issue in the past decade due to its impact on local economy, air quality, and public health
59 (Miettinen et al., 2011; Kunii et al., 2002; Frankenberg et al., 2005; Crippa et al., 2016;
60 Lee et al., 2018). Abundant aerosols emitted from such fires not only cause
61 environmental issues but also affect regional weather and climate through the direct and
62 indirect effects of biomass burning aerosols (Grandey et al., 2016; Hodzic and Duvel,
63 2017; Jeong and Wang, 2010; Ramanathan and Carmichael, 2008; Taylor, 2010; Tosca et
64 al., 2013). Carbonaceous compounds such as black carbon (BC) in biomass burning
65 aerosols can reduce sunlight through both absorption and scattering to warm the
66 atmosphere while cool the Earth’s surface (Fujii et al., 2014; Andreae and Gelencsér,
67 2006; Satheesh and Ramanathan, 2000; Ramanathan et al., 2001). Besides these direct
68 effects, biomass burning aerosols can act as cloud condensation nuclei or ice nuclei to
69 alter cloud microphysical structures and thus cloud radiation. Such “indirect effects” of
70 these aerosols on the climate are even more complicated due to various cloud and
71 meteorological conditions (Sekiguchi et al., 2003; Lin et al., 2013; Wu et al., 2013;
72 Grandey et al., 2016; Ramanathan et al., 2001; Wang, 2004).

73 For the Maritime Continent in Southeast Asia, convective precipitation associated
74 with the so-called Sumatra squall lines (SSL) and diurnal rainfall over Borneo is an
75 important weather feature (Lo and Orton, 2016; Ichikawa and Yasunari, 2006; Koh and
76 Teo, 2009; Yi and Lim, 2006; Wu et al., 2009). Convections of SSL are initially formed
77 in the northwestern side of Sumatra by the prevailing sea breezes from Indian Ocean and
78 the Sumatran mountain range, then propagate over the Malacca Strait affecting the Malay

79 Peninsula. Lo and Orton (2016) analyzed 22-year (1988 to 2009) ground-based Doppler
80 radar data and identified a total of 1337 squall lines in Singapore. They found that these
81 events with the diurnal cycle of rainfall most occur during either the summer monsoon
82 season (June-September) or the inter-monsoon periods (April-May and October-
83 November). Singapore, for example, experiences typically about 6~7 squall lines per
84 month during these periods. Oki and Musiake (1994) analyzed the seasonal and diurnal
85 cycles of precipitation using rain gauge data and showed that large-scale low-level winds
86 are a critical modulating factor in the diurnal cycle the convective rainfall over Borneo
87 besides the general reason of land-sea contrast behind convective rainfall in the Maritime
88 Continent. Furthermore, Ichikawa and Yasunari (2006) used five years Tropical Rainfall
89 Measuring Mission (TRMM) precipitation radar (PR) data to investigate the role of the
90 low-level prevailing wind in modulating the diurnal cycle of rainfall over Borneo. They
91 found that the diurnal cycle is associated with intraseasonal variability in the large-scale
92 circulation pattern, with regimes associated with either low-level easterlies or westerlies
93 over the island.

94 Interestingly, frequent biomass burning activities coincide with vigorous convective
95 systems in the Maritime Continent, especially during the summer monsoon season (June-
96 September), and could thus produce aerosols to affect convections in the region.
97 Rosenfeld (1999) analyzed TRMM data and hypothesized that abundant biomass burning
98 aerosols could practically shut off warm rain processes in tropical convective clouds.
99 Compared to the adjacent tropical clouds in the cleaner air, clouds encountered with
100 smokes could grow to higher altitudes with rain suppressed, hypothetically due to the
101 reduction of coalescence efficiency of smaller cloud drops into raindrops. Recently,

102 using Weather Research and Forecasting model with Chemistry (WRF-Chem), Ge et al.
103 (2014) have studied the direct and semi-direct radiative effects of biomass burning
104 aerosols over the Maritime Continent and found the radiative effect of biomass burning
105 aerosols could alter planetary boundary layer (PBL) height, local winds (including sea
106 breeze), and cloud cover. However, relative coarse resolution (27 km) adopted in their
107 simulation would not be able to reveal more details about how biomass burning aerosols
108 affect convective clouds through modifying cloud microphysics processes. Whereas,
109 Hodzic and Duvel (2017) have conducted a 40-day simulation using WRF-Chem with a
110 convection-permitting scale (4 km) to study the fire aerosol-convection interaction during
111 boreal summer in 2009 near the central Borneo mountainous region. Their result
112 suggests that modifications of the cloud microphysics by biomass burning aerosols could
113 reduce shallow precipitation in the afternoon and lead to a warm PBL anomaly at sunset,
114 all lead to an enforcement of deep convection at night. However, they have also
115 indicated that the radiative processes of moderately absorbing aerosols tend to reduce
116 deep convection over most regions due to local surface cooling and atmosphere warming
117 that increase the static stability, hence suggesting the complexity of the interaction of
118 biomass burning aerosols and convective clouds in the Maritime Continent.

119 In this study, we aim to examine and quantify the impacts of biomass burning
120 aerosols on convective systems over two targeted regions for analyses: the northern
121 Sumatra and the western Borneo in the Maritime Continent. Our focus is on not only the
122 change of hydrometeors in the convective clouds but also the change of rainfall amount
123 and intensity in these regions. We firstly describe methodologies adopted in the study,
124 followed by the results and findings from our numerical simulations over the Maritime

125 Continent. We have selected three cases in each study region to perform detail analyses.
126 In addition, statistical analyses covering the entire modeled fire season for each of these
127 two regions have also been performed to provide more generalized pictures about the
128 effects of fire aerosol on convection. The last section summarizes and concludes our
129 work.

130 **2 Methodology**

131 **2.1 Model and emission inventories**

132 In order to simulate trace gases and particulates interactively with the meteorological
133 fields, the Weather Research and Forecasting model coupled with a chemistry module
134 (WRF-Chem, see Grell et al. (2005)) version 3.6.1 is used in this study. Within WRF-
135 Chem, the Regional Acid Deposition Model, version 2 (RADM2) photochemical
136 mechanism (Stockwell et al., 1997) coupled with the Modal Aerosol Dynamics Model for
137 Europe (MADE) as well as the Secondary Organic Aerosol Model (SORGAM)
138 (Ackermann et al., 1998; Schell et al., 2001) are included to simulate atmospheric
139 chemistry and anthropogenic aerosol evolutions. MADE/SORGAM uses a modal
140 approach to represent the aerosol size distribution and predicts mass and number
141 concentrations of three aerosol modes (Aiken, accumulation, and coarse).

142 To resolve the convective system in the Maritime Continent in our simulations, two
143 model domains with two-way nesting are designed. Here, Domain 1 (431×141 grid
144 cells) has a resolution of 25 km, while Domain 2 (561×591 grid cells) has a resolution
145 of 5 km (Fig. 1). Specifically, Domain 1 is positioned to include the tropical Indian
146 Ocean on its west half in order to capture the path of Madden-Julian Oscillation (MJO),

147 and in the meantime to have a northern boundary constrained within 23°N in latitude to
148 avoid potential numerical instability from the terrain of Tibetan Plateau. Domain 2 with
149 a finer resolution is positioned to cover the mainland Southeast Asia as well as the islands
150 of Sumatra and Borneo.

151 The National Center for Environment Prediction FiNaL (NCEP-FNL) reanalysis
152 data (National Centers for Environmental Prediction, 2000) are used to provide initial and
153 boundary meteorological conditions, and to perform four-dimensional data assimilation
154 (FDDA) to nudge model temperature, water vapor, and zonal and meridional wind speeds
155 above the planetary boundary layer (PBL) for Domain 1. The time frequency of nudging
156 is every 6 hrs. The Mellor-Yamada-Nakanishi-Niino level 2.5 (MYNN) (Nakanishi and
157 Niino, 2009) is chosen as the scheme for planetary boundary layer in this study. Other
158 physics schemes adopted in the simulations include Morrison two-moment microphysics
159 scheme (Morrison et al., 2009), RRTMG longwave and shortwave radiation schemes
160 (Mlawer et al., 1997; Iacono et al., 2008), Unified Noah land-surface scheme (Tewari et
161 al., 2004), and Grell-Freitas ensemble cumulus scheme (Grell and Freitas, 2014) (for
162 Domain 1 only). Owing to the main purpose of this study to reveal fire aerosol-
163 convection interaction through modeling a large quantity of convective systems
164 continually over a relatively long period, and the computational resource available to us
165 as well, we have adopted a 5 km horizontal resolution which excluding cumulus
166 parameterization scheme. Previous studies have shown that WRF model with a similar
167 resolution without convection parameterization can still capture many critical
168 characteristics of deep convection (Wagner et al., 2018). Our model evaluation,

169 especially through the comparison of modeled results with sounding profiles, has
170 demonstrated the same.

171 WRF-Chem needs emissions for gaseous and particulate precursors to drive its
172 simulations. For this purpose, we have used the Regional Emission inventory in ASia
173 (REAS) version 2.1 (Kurokawa et al., 2013). REAS includes emissions of most primary
174 air pollutants and greenhouse gases, covering each month from 2000 to 2008. In
175 addition, the Fire INventory from U.S. National Center for Atmospheric Research
176 (NCAR) version 1.5 (FINNv1.5) (Wiedinmyer et al., 2011) is also used in the study to
177 provide biomass burning emissions. FINNv1.5 classifies burnings of extratropical forest,
178 tropical forest (including peatland), savanna, and grassland. Fire heat fluxes for four
179 different types of fire are prescribed in WRF-Chem to calculate the plume height (rf.
180 Table 1 in Freitas et al. (2007)). For peatland fire, we have set its heat flux as 4.4 kW m^{-2} ,
181 which is the same as that of savanna burning and differs from that of the tropical forest
182 burning in 30 kW m^{-2} . We modified the plume rise algorithm in WRF-Chem to
183 specifically improve the representation of tropical peat fire has been described in Lee et
184 al. (2017). It is worth indicating that the heat flux from biomass burning is not
185 incorporated in thermodynamic equation of current WRF-Chem model. Note that the
186 current fire emission inventories could underestimate near surface fire aerosol
187 concentration by ignoring some of the characteristics of smoldering burning as well (Shi
188 et al., 2019).

189 The default chemical profiles of several species in the lateral boundary condition are
190 higher than their background concentrations in our study region and thus equivalent to
191 provide additional aerosol sources from boundaries. To prevent this, we have set NO,

192 NO₂, SO₂, and all primary aerosol levels to zero at the lateral boundaries of Domain 1.
193 We have also adjusted the ozone profile used for lateral boundary condition based on the
194 World Meteorological Organization (WMO) Global Atmosphere Watch (GAW) station
195 in Bukit Kototabang, Indonesia (Lee et al., 2019).

196 **2.2 Numerical experiment design**

197 Two numerical simulations, both included anthropogenic emissions (mainly fossil
198 fuel emissions) while either with and without the biomass burning emissions (labeled as
199 FFBB and FF, respectively), have been conducted to investigate the impacts of biomass
200 burning aerosols on convective systems in the Maritime Continent through both direct
201 and indirect effects. Our study focuses on the fire season from June to September of
202 2008. Therefore, the simulations start from 1 May of 2008 and last for five months. The
203 first month is used as a spin-up period. Among the years with available emission data,
204 both emission amount of biomass burning and total precipitation in 2008 approximate
205 their ensemble mean or represent an average condition (Fig. S1). Nevertheless,
206 interannual variation of biomass burning emissions alongside precipitation in the studies
207 regions do exist (Lee et al., 2017; Lee et al., 2018), and the influence of such variation on
208 the effects of fire aerosol on convection should be addressed in future studies.

209 **2.3 Analysis methods**

210 The primary target of this study is the convective systems associated with Sumatra
211 squall lines and diurnal rainfall over Borneo. Thus, our analyses mainly focus on the
212 convections over two specific regions: the Sumatra region (r1 in Fig. 1) and the Borneo
213 region (r2 in Fig. 1). The area coverage of the Sumatra region (r1) is from 97° to 103° E

214 in longitude and 0° to 6° N in latitude, while the area coverage of the Borneo region (r2)
215 is from 109° to 115° E in longitude and 1° S to 5° N in latitude.

216 To examine the impacts of fire aerosols on cloud formation and rainfall intensity as
217 well as amount, we have selected three convective systems each for the two focused
218 regions to perform an in-depth case study. We first trace the path of individual
219 convections and focus the analyses on the specific area of each of these convective
220 systems to identify the impacts of fire aerosols. Table 1 shows the selected cases in the
221 Sumatra region (r1) and the Borneo region (r2). The selected cases are chosen randomly
222 from different fire periods of the two study regions. We did not set any criteria initially
223 when we chose these cases. After we analyzed all cases, 3 mm 3hr⁻¹ was set as the
224 threshold to distinguish weak and strong convections.

225 The consequent analyses are then focused on the fire-season-wise statistics of
226 convections for each study region. Table 2 and Fig. S2 show the fire periods in the two
227 study regions. There are total of 54 convective systems simulated during the fire periods
228 in the Sumatra region (r1) and 35 convective systems in the Borneo region (r2).

229 The statistical quantities used in this study follows Wang (2005) to estimate the
230 mean value over a specific region (e.g., r1 or r2). The cloud area mean quantities are
231 defined as a function of output time step (t) by the following equation:

$$232 \quad \bar{c}^{area}(t) = \frac{1}{N(t)} \sum_{\substack{q > q_{min} \\ n > n_{min}}} c(x, y, z, t). \quad (1)$$

233 Here c is a given quantity (e.g., cloud water mass). Eq. (1) only applies to the grid points
234 where both the mass concentration q and number concentration n of a hydrometeor
235 exceed their given minima. The total number of these grid points at a given output time
236 step t is represented by $N(t)$. The cloud area mean quantities are used to present the

237 average quantities of a given variable at a given output time step. Note that the cloud
238 area mean quantities only apply to hydrometeors. For rainfall, the analyzed quantities are
239 spatial averages over a specific area of the convective system for case study or over the
240 entire study region for longer-term statistic estimate.

241 **3 Results**

242 **3.1 Model evaluation**

243 **3.1.1 Precipitation**

244 The satellite-retrieved precipitation of the Tropical Rainfall Measuring Mission
245 (TRMM) 3B42 3hrly (V7) dataset (Huffman et al., 2007) is used in this study to evaluate
246 simulated rainfall. Figure 2a and 2b show the Hovmöller plots of daily TRMM and
247 FFBB precipitation from 1 June 2008 to 30 September 2008, respectively. Compared to
248 the satellite-retrieved data, the model has captured all the major rainfall events in the two
249 analysis regions (Fig. 3). In addition, because of its higher spatial resolution than
250 TRMM, the model produces more light rain events. Nevertheless, as indicated in our
251 previous study (Lee et al., 2017), a wet bias of the model is evident and mainly comes
252 from water vapor nudging in data assimilation (FDDA). As a result, the daily average
253 rainfall in FFBB over the Sumatra region (r1) is 11.05 ± 5.90 mm day⁻¹ from 1 June 2008
254 to 30 September 2008, higher than that of 7.21 ± 5.54 mm day⁻¹ derived from TRMM
255 retrieval. The wet bias also exists in the modeling results in the Borneo region (r2),
256 where daily average rainfall there is 15.40 ± 8.49 mm day⁻¹ in FFBB and only 9.56 ± 7.20
257 mm day⁻¹ in TRMM. For the simulated rainfall in FFBB, the temporal correlation with
258 TRMM is 0.44 in the Sumatra region (r1) and 0.64 in the Borneo region (r2).

259 **3.1.2 Aerosol optical depth (AOD)**

260 Because of limited ground-based observational data of aerosols, we use Aerosol
261 Optical Depth (AOD) from the level-3 Moderate Resolution Imaging Spectroradiometer
262 (MODIS) gridded atmosphere monthly global joint product (MOD08_M3;
263 http://dx.doi.org/10.5067/MODIS/MOD08_M3.061) to evaluate modeled aerosol spatial
264 distribution and relative concentration. Figure 4a shows MODIS monthly AOD in
265 Southeast Asia in September 2008. High AOD occurs in the southern part of Sumatra
266 and the southwestern part of Borneo. Compared to the MODIS retrieval, the modeled
267 AOD in FFBB has similar spatial distribution but a higher value (Fig. 4b). It is because a
268 high spatiotemporal resolution in our simulation enables the model to capture episodic
269 fire events better. In contrast, FF simulation produces much lower AOD values than
270 those of MODIS and FFBB, thus suggesting biomass burning aerosols make a substantial
271 fraction in atmospheric AOD during burning seasons.

272 **3.1.3 Sounding profiles**

273 We have used multiple weather sounding profiles measured in Bintulu Airport,
274 Malaysia (113.03° E, 3.20° N), provided by University of Wyoming
275 (<http://weather.uwyo.edu/upperair/sounding.html>). An example for detailed summary is
276 a case at 12 UTC on 22 September 2008 (Fig. 5a). This sounding provides information
277 of atmospheric state (e.g., vertical distributions of pressure, temperature, wind speed,
278 wind direction, and humidity) coinciding with one of our selected case study (r2c3) of
279 diurnal convective rainfall in Borneo. Compared to the observed sounding data, the
280 FFBB simulation has produced similar temperature and wind profiles and well captured

281 the low-level and high-level wind speeds and wind directions (Fig. 5a versus 5b). It also
282 well predicts several key indexes of convection: temperature and pressure of the Lifted
283 Condensation Level (LCL) simulated in FFBB are 296.2 K and 955 hPa, respectively,
284 which are close to the values of 296.2 K in temperature and 960.7 hPa in pressure derived
285 from the observed sounding data. The model predicts 3049 J of Convective Available
286 Potential Energy (CAPE), while 2031 J of CAPE is estimated in the observed sounding
287 data. Besides this 22 September 2008 case, the model has also captured major features of
288 observed profiles for all the other cases selected in our analyses shown in Fig. S3~S7.

289 **3.1.4 Cloud vertical structure**

290 The Cloud-Aerosol Lidar and Infrared Pathfinder Satellite Observation (CALIPSO)
291 provides information of the vertical structure of clouds on its path around the globe
292 (https://www-calipso.larc.nasa.gov/products/lidar/browse_images/production/), including
293 that of one of our cases (r2c3) of diurnal convective rainfall in Borneo on 22 September,
294 2008 (Fig. 6a). For this case, CALIPSO shows the vertical structure of a convective
295 system over Borneo along with high PM_{2.5} concentration near the surface (yellowish
296 color near the surface), implying a potential impact of biomass burning aerosols on
297 convective clouds. It can be seen that the FFBB simulations well captures the vertical
298 structure of convective clouds as well as the near-surface aerosol layers, including their
299 vertical extension (Fig. 6c versus 6a). With the comparison of FF simulation, we are able
300 to identify the biomass burning origin of these aerosols near the surface. It is worth to
301 indicate that we have compared more than 50 modeled convections during the fire season
302 and within the simulation domains. However, the others captured by CALIPSO are

303 either not among the selected cases or are mostly out of our analyzed domains, so we did
304 not have further discussion here.

305 **3.2 Analyses of selected cases in two study regions**

306 **3.2.1 The Sumatra region (r1)**

307 The three selected cases in r1 or the Sumatra region (r1c1, r1c2 and r1c3) all
308 occurred in the afternoon (2 PM or 5 PM local time) and lasted less than 24 hours (Table
309 1). The sounding profile of three cases show quite similar to the environmental profiles
310 (Fig. S3~S5). Most fire aerosols in this study region were initially emitted from the
311 central and south Sumatra then transported along with southwesterly winds to encounter
312 convections in the northern Sumatra. Compared to the result of FF, PM_{2.5} concentration
313 in FFBB can be 6~12 times higher in the Sumatra region (r1) in these selected cases (Fig.
314 7).

315 Aerosols from biomass burning in FFBB add 2~3 times more cloud droplet number
316 concentration and 8~20% higher cloud water mass compared to the results in FF (Table
317 2). The mean radius of cloud droplets in FFBB is about 6~7 μm , clearly smaller than that
318 in FF (10~11 μm). Smaller cloud droplet in FFBB reduces the efficiency of
319 autoconversion, and further decreases rain water mass and raindrop number
320 concentration. Hence, raindrop number concentration in FFBB is 40~50% lower than
321 that in FF among our selected cases in r1 (Table 3). However, besides autoconversion,
322 rain water mass is also affected by other microphysics processes. Larger raindrops
323 combining with smaller cloud droplets in FFBB can enhance the efficiency of cloud
324 droplet collection by rain and thus increase rain water mass but cause no change to the

325 number of raindrops, possibly compensating the decrease of rain water mass resulted
326 from a lowered autoconversion. Overall, rain water mass decreases 15% in the case of
327 r1c2 and 10% in the case of r1c3, respectively. Compared to the cases of r1c2 and r1c3,
328 the case of r1c1 is a relatively weak convective system based on a threshold of ~ 3 mm
329 3hr^{-1} of the averaged rainfall in FF (Table 4). After introducing fire aerosols, the mass
330 concentration of snow and graupel in this case increases 62% and 48%, respectively.
331 Melting snow and graupel in the lower atmosphere results in a significant increase of rain
332 water mass concentration by 49%. Thus, total hydrometeor mass is increased by 36% in
333 FFBB from that in FF. Our result is consistent with that of Lin et al. (2006), which
334 suggested that biomass burning aerosols could invigorate convection and then increase
335 precipitation based on satellite observations. The aerosol invigoration effect is referred to
336 such a hypothetic process that increasing number of smaller cloud droplets due to higher
337 aerosol concentration would reduce the efficiency of raindrop formation from self-
338 collection among cloud droplets, and thus further slowdown the loss of these small
339 droplets from being collected by larger raindrops and allow more of them reach high
340 altitudes, where they would eventually collected by ice particles through riming, causing
341 release of latent heat to enhance updraft (Rosenfeld et al., 2008). For tropical regions
342 with high humidity, additional aerosols may also lead to the warm-phase invigoration due
343 to the consequent enhancement in total condensed water quantity and thus latent heat
344 release (Wang, 2005; Fan et al., 2018). Note that the “aerosol-aware” microphysics
345 scheme in WRF-Chem only applies to the warm cloud process (Morrison et al., 2005;
346 Morrison et al., 2009); therefore, ice nucleation is parameterized of ambient temperature
347 only regardless of the aerosol concentration. In our model configuration, fire aerosol can

348 still affect ice process, however, through CCN effect rather than serving directly as ice
349 nuclei.

350 In the FF simulations, the convective system in the case of r1c2 and r1c3 is stronger
351 than the system in the case of r1c1, and the average rainfall of r1c2 and r1c3 is also
352 higher than the rainfall of r1c1 (Table 4). Adding fire aerosols in FFBB does not
353 substantially change the average rainfall in r1c2 and r1c3 (+3% and -8%, respectively;
354 Table 4). However, in the relatively weak convective system of r1c1, adding fire
355 aerosols significantly increases the mean rainfall amount by 106% ($1.33 \pm 0.47 \text{ mm } 3\text{hr}^{-1}$
356 in FF versus $2.74 \pm 1.21 \text{ mm } 3\text{hr}^{-1}$ in FFBB).

357 **3.2.2 The Borneo region (r2)**

358 The three selected cases in r2 (r2c1, r2c2, and r2c3) also occurred during the summer
359 monsoon season when active biomass burning events existed in the west Borneo. In
360 these cases, fire aerosols were transported to the north and northeast by the southeasterly
361 and southwesterly winds. Because of the proximity of fire emissions, the $\text{PM}_{2.5}$
362 concentration in FFBB can be 24 times higher than that in FF in the Borneo region (r2) in
363 these selected cases (Fig. 7).

364 The modeled results demonstrate the substantial impacts of fire aerosols on both
365 ambient aerosol concentration and cloud droplet number concentration. $\text{PM}_{2.5}$
366 concentration in FFBB is drastically higher than that in FF with the highest increase
367 appears in the case of r2c1 at 4940%, more than doubled the values of r2c2 (2402%) and
368 r2c3 (2422%). The increase in cloud droplet number concentration in the case of r2c1
369 (703%) is also substantially higher than those in r2c2 (337%) and r2c3 (409%) (Table 2).

370 The mean radius of cloud droplets in FFBB is about 6~7 μm , which is significantly
371 smaller than that in FF (10~11 μm). The mean cloud droplet radii in FF and FFBB in r2
372 are similar to the results in r1. On the other hand, the increase of cloud water mass due to
373 fire aerosols is not so dramatic in all these cases, only about 8%~27% higher than that in
374 the FF simulations (Table 3). As discussed above, rain number concentration in FFBB
375 over the Borneo region (r2) is lower than that in FF, similar to the cases in r1, likely due
376 to the low efficiency of autoconversion induced by the presence of a large quantity of
377 smaller cloud droplets. Rain water mass of FFBB in the r2c1 case is decreased by about
378 6% due to fire aerosols, which is similar to the results in the r1c2 and r1c3 cases over the
379 Sumatra region (Table 3). However, interestingly, rain water and snow mass are both
380 increased in FFBB by 64% and 69% in r2c2 and by 19% and 60% in r2c3, respectively
381 (Table 3). The cases of r2c2 and r2c3 are relatively weak convective systems, similar to
382 the case of r1c1. Again, it is based on based on a threshold of $\sim 3 \text{ mm } 3\text{hr}^{-1}$ of the
383 averaged rainfall in FF (Table 4). Our results show that fire aerosols have substantial
384 impacts on cold cloud processes in the weak convective systems. Overall, total
385 hydrometeor mass concentration in FFBB have increased 47% in r2c2 and 13% in r2c3.

386 The changes of rainfall amount due to fire aerosols in r2 are similar to the cases in r1.
387 For the strong convection case of r2c1, adding fire aerosols in the FFBB simulation
388 decreases the total rainfall amount by 18%. However, in the weak convection cases of
389 r2c2 and r2c3, adding fire aerosols would double the rainfall amount (Table 4).
390 Compared to the results in FF, rainfall intensity is persistently higher in FFBB during the
391 convection life cycle in those weak convection cases. Nighttime rainfall intensity in
392 FFBB, especially, is much higher than the rainfall intensity in FF. Therefore, as shown

393 by our results, fire aerosols appear to have more substantial impacts on the quantities of
394 hydrometeors and rainfall of the weak convection cases in both Sumatra region (r1) and
395 Borneo region (r2).

396 Our results show that fire aerosols tend to invigorate weak convection but suppress
397 deep convection in both Sumatra region (r1) and Borneo region (r2). As mentioned
398 before, increasing the number of smaller cloud droplets due to higher aerosol
399 concentration resulted from fire would reduce the efficiency of raindrop formation
400 through the warm-rain processes, thus allowing more cloud droplets reach high altitudes
401 to be eventually collected by ice particles through riming, causing release of latent heat to
402 invigorate updraft while enhancing precipitation through melting of fallen ice particles
403 (Wang, 2005). These processes appear to be more effective to weak convections than
404 deep convections and were in fact well-simulated in the former cases. The results are
405 also consistent with some previous observation-based studies (Jiang et al., 2018; Zhao et
406 al., 2018). Jiang et al. (2018) and Zhao et al. (2018) both concluded that an increase of
407 fire aerosols generally reduces cloud optical thickness of deep convection while Zhao et
408 al. (2018) further showed that fire aerosols tend to invigorate weak convection for small-
409 to-moderate aerosol loadings.

410 **3.3 Fire-season statistics of convections in two study regions**

411 Statistics covering the entire simulated fire season (~4 months) for each study region
412 have been derived to provide trend/tendency information regarding several aspects of the
413 impact of fire aerosols on convections. In our simulations, $PM_{2.5}$ concentration in FF
414 during the fire periods, which can be regarded as the background value for FFBB

415 simulation before adding fire aerosols, is $1.36 \pm 0.19 \mu\text{g m}^{-3}$ in r1 and $0.56 \pm 0.09 \mu\text{g m}^{-3}$ in
416 r2. In comparison, $\text{PM}_{2.5}$ concentration in FFBB is $11.37 \pm 10.41 \mu\text{g m}^{-3}$ in r1 and
417 $10.07 \pm 7.73 \mu\text{g m}^{-3}$ in r2. Note that unlike in some other studies where the control
418 simulations use constant aerosol concentrations, fire aerosol concentrations in our
419 simulations can vary in responses to changes in fire emissions, or aerosol removal by rain
420 scavenging due to precipitation change caused by fire aerosols themselves. Hence, the
421 processes included in our simulations are closer to reality, and the results could better
422 reflect the nature of fire aerosol-convection interaction in the Maritime Continent.

423 Averaged through the entire modeled fire periods, cloud water mass (Q_c), cloud
424 droplet number concentration (Q_{nc}), and rain drop number concentration (Q_{nr}) in FFBB
425 differ substantially from those in FF, demonstrating the influence of fire aerosols. Figure
426 8 shows that adding fire aerosols in FFBB would increase Q_c by 14% and Q_{nc} by 226%
427 in r1, and Q_c by 18% and Q_{nc} by 349% in r2. Another pronounced change in response to
428 adding fire aerosols is a decrease in Q_{nr} by 44% in r1 and 47% in r2. Although an
429 increase in snow mass (Q_s) and graupel mass (Q_g) and a decrease in rain water mass (Q_r)
430 after adding fire aerosols, the uncertainty of these hydrometeor changes is large.

431 In Sect. 3.2, we have discussed the significant rainfall increase occurred in the weak
432 convective systems after adding fire aerosols due to aerosol invigoration effect. On one
433 hand, regardless the strength of convection, the mean 3-hourly rainfall during the fire
434 periods is $1.06 \pm 0.85 \text{ mm}$ in FF and $1.09 \pm 0.86 \text{ mm}$ in FFBB over the Sumatra region (r1),
435 and statistically it does not change significantly in responding to fire aerosols. The
436 rainfall difference in the Borneo region (r2) between FF and FFBB is also insignificant
437 ($1.32 \pm 1.20 \text{ mm 3hrs}^{-1}$ in FF versus $1.35 \pm 1.14 \text{ mm 3hrs}^{-1}$ in FFBB). On the other hand,

438 we have found that the impacts of fire aerosols appear in several other rainfall patterns.
439 For instance, the daily maximum and minimum rainfalls display clear differences
440 between the FFBB and FF simulations, specifically in r2 rather than in r1 (Fig. 9). While
441 for r1, the impacts of fire aerosol are reflected in event-wise statistics, e.g., higher event-
442 wise maximum and minimum rainfall intensity in FFBB than in FF, identified in 30 out
443 of 54 convective events in total. These are mostly weak convective events in r1.
444 Interestingly, somewhat opposite to the rainfall statistics in r1, the intensity of event-wise
445 maximum and minimum rainfall in r2 is higher in FF than in FFBB. The daily rainfall
446 peak of 3-hr rainfall in r1 is mostly less than 3 mm; in comparison, one-third of
447 convective events in r2 have daily maximum 3-hr rainfall exceeding 3 mm (Fig. 9c),
448 suggesting that the convective systems in r2 tend to develop stronger than in r1 and the
449 fire aerosols significantly suppress the maximum rainfall intensity of strong convections
450 in r1. We roughly used $1.25 \text{ mm } 3\text{hr}^{-1}$ of the domain-averaged rainfall to classify weak
451 and strong convective systems. We find that the conclusions regarding differences of
452 hydrometers and rainfall in the weak systems between the FF and FFBB experiments stay
453 the same, and such differences are still not that significant in both regions (Table S1 and
454 Fig. S8).

455 We have categorized the maximum rainfall based on its values in the afternoon and
456 midnight. We find that those heavy maximum rainfalls in r2 tend to occur in the
457 midnight (Fig. 9c) associated with the anticyclonic circulation formed in the western
458 Borneo induced by southeasterly winds from the Southern latitude turn northeastward
459 along the west coast of Borneo, owing to the terrain of Borneo Island and the sea breezes
460 from the South China Sea. The vortex produced by such a circulation leads to strong

461 updraft and then strong convection. Note that this anticyclonic circulation is different
462 from the Borneo vortex, the latter appears as a persistent feature of the boreal winter
463 climatology and is related to the northeasterly from the South China Sea and cold surge
464 events (Chang et al., 1983; Chang et al., 2005).

465 The low-level wind pattern of Borneo convections is similar to the westerly regime,
466 especially the weak westerly (WW) regime identified by Ichikawa and Yasunari (2006).
467 According to their analysis, the WW regime tends to occur in boreal summer. Its
468 composites include an anticyclonic feature with the weak wind field over the Borneo
469 Island. The deep convective storms developed in the WW regime tend to stay close to
470 the west coast associated with the lower-level convergence enhanced by the prevailing
471 wind and local circulations around there, resulting in localized rainfall over the offshore
472 region of the west coast. Based on our simulations, the onset of convection occurs in the
473 afternoon over the western mountain range of Borneo. These storms would consequently
474 evolve into widespread shallow storms in the evening over the western part of the island.
475 The maximum rainfall appears on the west coast because of a local westward propagating
476 rainfall system that develops around midnight or early morning.

477 The comparison of the maximum rainfall between FF and FFBB in Fig. 9 shows that
478 fire aerosols tend to reduce the maximum rainfall, especially for high-intensity rainfall
479 events. In other words, fire aerosols have substantial impacts on the nocturnal
480 convections, which are associated with the local anticyclonic circulation in the western
481 Borneo. This effect on nocturnal convections in the western Borneo by fire aerosols will
482 be discussed further in the next section.

483 **3.4 The impact of biomass burning aerosols on nocturnal**
484 **convections in the Borneo region**

485 To further analyze the effects of fire aerosols on nocturnal convections, we have
486 categorized convective events into nocturnal convections (NC) and non-nocturnal
487 convections (non-NC), based on whether the maximum rainfall occurs from midnight to
488 early morning or in the time frame from late afternoon to evening. Figure 10 shows the
489 diurnal time series of precipitation averaged over the Borneo region (r_2) in FF and FFBB.
490 Again, 3-hour-mean rainfalls of nocturnal convections are higher than those of non-
491 nocturnal convections in both simulations and fire aerosols weaken the maximum
492 nocturnal rainfall intensity about 9%.

493 Nocturnal convections tend to stay close to the west coast associated with a lower-
494 level convergence enhanced by the prevailing wind and local circulations mainly related
495 to the land breezes from inland of the western Borneo. The strong convergence near the
496 surface over the offshore region of the west coast causes the weak westerly monsoon
497 windflaws and local land breezes to merge during the nighttime. However, during the
498 fire periods, the daytime absorption of fire aerosols (e.g., black carbon) can cause an
499 atmospheric warming (even without fire generated heating flux being incorporated in the
500 model). This could increase near surface air temperature, weaken land breezes and thus
501 surface convergence. As a result, the nocturnal convections in FFBB cannot develop as
502 strong as those in FF. On the other hand, both nocturnal and non-nocturnal convections
503 are initiated over the western mountain range under a prevailing wind of the sea breezes
504 from the South China Sea. The increases of near surface temperature owing to the fire

505 aerosols can enhance this prevailing wind from the ocean and thus lead to a higher
506 convective rainfall in FFBB during the onset stage of the nocturnal convections as well as
507 non-nocturnal convections. Figure 11 illustrates the sea breeze increase in FFBB during
508 the daytime (20 LST) and the land breeze decrease in FFBB during the nighttime (2
509 LST). Twenty LST and 2 LST are chosen here because of the peak of difference.

510 Diurnal evolution of vertical profiles clearly indicates that mass mixing ratio of total
511 hydrometeors, temperature, and vertical velocity differ in both daytime and nighttime
512 between FF and FFBB for those nocturnal convections (Fig. 12). The differences of near
513 surface temperature between FF and FFBB are more pronounced during the period after
514 sunset (Fig. 12d). The differences of near surface temperature mainly happen over land,
515 and the higher near surface temperature in FFBB weakens the land breezes and near
516 surface convergence along the coast. Starting from late afternoon, (about 5 PM local
517 time), vertical velocity increases with time until sunrise next day in both simulations (Fig.
518 12e) due to the convergence of the monsoon windflaws and local land breezes during the
519 nighttime, and this matches very well with that of mass mixing ratio of total
520 hydrometeors (Fig. 12a and 12e). Noticeably, the main differences in vertical velocity
521 and hydrometeor mass mixing ratio between FFBB and FF also start to become evident
522 after entering the evening. Because of the weaker convergence near the surface in FFBB,
523 the differences in vertical velocity at the higher altitude between FFBB and FF peaks in
524 the nighttime. The temperature increase from aerosol absorption seems small (please
525 note that the direct heating from fire is not included in the WRF fire plume model) but we
526 do see the change of vertical velocity owing to the aerosol heating effect. Based on our
527 analysis, the temperature increase is mainly associated with the thermodynamic

528 perturbation from the absorption of sunlight by fire aerosols. This seems also consistent
529 with the analysis of Zhang et al. (2019). Indeed, should the heat flux generated by fires
530 be incorporated in the model, the warming effects from biomass burning would be much
531 stronger and also persist in nocturnal timeframe.

532 As a summary, the schematics shown in Fig. 13 illustrate the impact of biomass
533 burning activities on nocturnal convections in the Borneo region. In the daytime, under
534 the prevailing wind of sea breezes from the South China Sea, convections develop over
535 the western mountain range. Because near surface heating from the absorption of
536 sunlight by fire aerosols could enhance the prevailing wind from the ocean, convective
537 rainfall becomes higher at the onset stage of the nocturnal convections (still in daytime)
538 due to biomass burning activities (Fig. 13b). In the nighttime, convection moves to the
539 offshore region of the western Borneo. The strong convergences near the surface merge
540 the weak westerly monsoon windflaws with local nighttime land breezes to form an
541 anticyclonic circulation (Fig. 13c). During the fire periods, the daytime near surface
542 warming by fire aerosols could also further weaken land breezes and surface
543 convergence. Hence, the nocturnal convections during fire events would not develop as
544 strong as in days without fires (Fig. 13d versus 13c).

545 **4 Summary**

546 By comparing WRF-Chem modeling results include or exclude biomass burning
547 emissions (FFBB versus FF), we have identified certain detailed impacts of fire aerosols
548 on convective events within two study regions in the Maritime Continent during a four-
549 month period (June 2008 ~ September 2008). In total, 54 convective systems in the

550 Sumatra region and 35 convective systems in the Borneo region have been simulated.
551 Three convective events of each study region have been selected for in-depth
552 investigation. In addition, statistical analyses have been performed throughout the entire
553 simulation period for each region. We have focused our analyses on two rainfall
554 features: 1) convective precipitation associated with Sumatra squall lines, and 2) diurnal
555 rainfall over the western Borneo.

556 We find that fire aerosols lead to the increase of cloud water mass and cloud droplet
557 number concentration among all analyzed cases while a substantial reduction of rain drop
558 number concentration. Influences of fire aerosols on other hydrometeors vary from case
559 to case. Specifically, our results show that fire aerosols can significantly change the
560 quantities of hydrometeors, particularly those involved in cold cloud processes and
561 rainfall of weak convections in either the Sumatra region or the Borneo region. Rainfall
562 intensity is higher in FFBB during the entire convection life cycle in those weak
563 convection cases, and the nighttime rainfall intensity in FFBB is significantly higher than
564 that in FF.

565 Statistics performed throughout the entire modeled fire season shows that the fire
566 aerosols only cause a nearly negligible change (2-3%) to the total rainfall of convective
567 systems in both study regions. On the other hand, we notice that fire aerosols can still
568 alter daily maximum and minimum rainfall in some cases, for example, fire aerosols lead
569 to the increase of maximum and minimum rainfall intensity in 30 weak convective events
570 in the Sumatra region.

571 In the Borneo region, biomass burning activities mainly affect the rainfall intensity
572 of nocturnal convection. Because near surface heating from the absorption of fire

573 aerosols can enhance the prevailing wind from the ocean (sea breeze) during the daytime,
574 the convective rainfall over the western mountain range is higher during the onset stage
575 of the nocturnal convections. In the nighttime, the consequence of the above
576 thermodynamic perturbation by absorbing fire aerosols can further weaken land breeze
577 and surface convergence. Hence, the rainfall intensity of nocturnal convections under the
578 influence of fire aerosols would become weaker by about 9%.

579 This study has demonstrated how biomass burning activities could affect convective
580 systems in the Maritime Continent by altering cloud microphysics and dynamics. We
581 find the biomass burning activities significantly change the diurnal rainfall intensity,
582 especially those low-level wind patterns associated with the weak westerly (WW) regime
583 as suggested by Ichikawa and Yasunari (2006). Our results show that neither a single
584 case study nor a simple statistical summary applied to overall model simulation period
585 without in-depth analyses could reveal the impact of biomass burning aerosols on
586 convections under different windflow regimes.

587 **Data availability**

588 FINNv1.5 emission data are publicly available from
589 <http://bai.acom.uar.edu/Data/fire/>. REAS emission data can be downloaded from
590 <https://www.nies.go.jp/REAS/>. TRMM data can be obtained from
591 <https://pmm.nasa.gov/data-access/downloads/trmm>. AOD from MODIS can be
592 obtained from http://dx.doi.org/10.5067/MODIS/MOD08_M3.061. Sounding profiles
593 are publicly available on <http://weather.uwyo.edu/upperair/sounding.html>. WRF-Chem
594 simulated data are available upon request from Hsiang-He Lee (lee1061@llnl.gov).

595 **Author contribution**

596 H.-H. L. and C. W. designed the experiments and H.-H. L. carried them out. H.-H.
597 L. configured the simulations and analyzed the results. H.-H. L. and C. W. wrote the
598 manuscript.

599 **Acknowledgments**

600 This research was supported by the National Research Foundation Singapore through
601 the Singapore-MIT Alliance for Research and Technology, the interdisciplinary research
602 program of Center for Environmental Sensing and Modeling. It was also supported by
603 the U.S. National Science Foundation (AGS-1339264) and L'Agence National de la
604 Recherche (ANR) of France through the Make-Our-Planet-Great-Again Initiative, ANR-
605 18-MPGA-003 EUROACE. The authors would like to acknowledge NCEP-FNL and
606 NCAR FINN working groups for releasing their data to the research communities; and
607 the NCAR WRF developing team for providing the numerical model for this study. The
608 computational work for this article was performed on resources of the National
609 Supercomputing Centre, Singapore (<https://www.nscg.sg>).

610

611

612

613

614

615 **Reference:**

- 616 Ackermann, I. J., Hass, H., Memmesheimer, M., Ebel, A., Binkowski, F. S., and
617 Shankar, U.: Modal aerosol dynamics model for Europe: development and first
618 applications, *Atmospheric Environment*, 32, 2981-2999,
619 [http://dx.doi.org/10.1016/S1352-2310\(98\)00006-5](http://dx.doi.org/10.1016/S1352-2310(98)00006-5), 1998.
- 620 Andreae, M. O., and Gelencsér, A.: Black carbon or brown carbon? The nature of
621 light-absorbing carbonaceous aerosols, *Atmos. Chem. Phys.*, 6, 3131-3148,
622 10.5194/acp-6-3131-2006, 2006.
- 623 Chang, C.-P., Millard, J. E., and Chen, G. T. J.: Gravitational Character of Cold
624 Surges during Winter MONEX, *Monthly Weather Review*, 111, 293-307,
625 10.1175/1520-0493(1983)111<0293:gcoocsd>2.0.co;2, 1983.
- 626 Chang, C.-P., Harr, P. A., and Chen, H.-J.: Synoptic Disturbances over the
627 Equatorial South China Sea and Western Maritime Continent during Boreal Winter,
628 *Monthly Weather Review*, 133, 489-503, 10.1175/mwr-2868.1, 2005.
- 629 Crippa, P., Castruccio, S., Archer-Nicholls, S., Lebron, G. B., Kuwata, M., Thota, A.,
630 Sumin, S., Butt, E., Wiedinmyer, C., and Spracklen, D. V.: Population exposure to
631 hazardous air quality due to the 2015 fires in Equatorial Asia, *Scientific Reports*, 6,
632 37074, 10.1038/srep37074, 2016.
- 633 Fan, J., Rosenfeld, D., Zhang, Y., Giangrande, S. E., Li, Z., Machado, L. A. T., Martin,
634 S. T., Yang, Y., Wang, J., Artaxo, P., Barbosa, H. M. J., Braga, R. C., Comstock, J. M., Feng,
635 Z., Gao, W., Gomes, H. B., Mei, F., Pöhlker, C., Pöhlker, M. L., Pöschl, U., and de Souza,
636 R. A. F.: Substantial convection and precipitation enhancements by ultrafine aerosol
637 particles, *Science*, 359, 411-418, 10.1126/science.aan8461, 2018.
- 638 Frankenberg, E., McKee, D., and Thomas, D.: Health consequences of forest fires
639 in Indonesia, *Demography*, 42, 109-129, 10.1353/dem.2005.0004, 2005.
- 640 Freitas, S. R., Longo, K. M., Chatfield, R., Latham, D., Silva Dias, M. A. F., Andreae,
641 M. O., Prins, E., Santos, J. C., Gielow, R., and Carvalho Jr, J. A.: Including the sub-grid
642 scale plume rise of vegetation fires in low resolution atmospheric transport models,
643 *Atmos. Chem. Phys.*, 7, 3385-3398, 10.5194/acp-7-3385-2007, 2007.
- 644 Fujii, Y., Iriana, W., Oda, M., Puriwigati, A., Tohno, S., Lestari, P., Mizohata, A., and
645 Huboyo, H. S.: Characteristics of carbonaceous aerosols emitted from peatland fire in
646 Riau, Sumatra, Indonesia, *Atmospheric Environment*, 87, 164-169,
647 <http://dx.doi.org/10.1016/j.atmosenv.2014.01.037>, 2014.
- 648 Ge, C., Wang, J., and Reid, J. S.: Mesoscale modeling of smoke transport over the
649 Southeast Asian Maritime Continent: coupling of smoke direct radiative effect below
650 and above the low-level clouds, *Atmos. Chem. Phys.*, 14, 159-174, 10.5194/acp-14-
651 159-2014, 2014.
- 652 Grandey, B. S., Lee, H. H., and Wang, C.: Radiative effects of interannually varying
653 vs. interannually invariant aerosol emissions from fires, *Atmos. Chem. Phys.*, 16,
654 14495-14513, 10.5194/acp-16-14495-2016, 2016.
- 655 Grell, G. A., Peckham, S. E., Schmitz, R., McKeen, S. A., Frost, G., Skamarock, W. C.,
656 and Eder, B.: Fully coupled "online" chemistry within the WRF model, *Atmospheric
657 Environment*, 39, 6957-6975, 10.1016/j.atmosenv.2005.04.027, 2005.

658 Grell, G. A., and Freitas, S. R.: A scale and aerosol aware stochastic convective
659 parameterization for weather and air quality modeling, *Atmos. Chem. Phys.*, 14,
660 5233-5250, 10.5194/acp-14-5233-2014, 2014.

661 Hodzic, A., and Duvel, J. P.: Impact of Biomass Burning Aerosols on the Diurnal
662 Cycle of Convective Clouds and Precipitation Over a Tropical Island, *Journal of*
663 *Geophysical Research: Atmospheres*, 123, 1017-1036, 10.1002/2017JD027521,
664 2017.

665 Huffman, G. J., Bolvin, D. T., Nelkin, E. J., Wolff, D. B., Adler, R. F., Gu, G., Hong, Y.,
666 Bowman, K. P., and Stocker, E. F.: The TRMM Multisatellite Precipitation Analysis
667 (TMPA): Quasi-Global, Multiyear, Combined-Sensor Precipitation Estimates at Fine
668 Scales, *Journal of Hydrometeorology*, 8, 38-55, 10.1175/JHM560.1, 2007.

669 Iacono, M. J., Delamere, J. S., Mlawer, E. J., Shephard, M. W., Clough, S. A., and
670 Collins, W. D.: Radiative forcing by long-lived greenhouse gases: Calculations with
671 the AER radiative transfer models, *Journal of Geophysical Research: Atmospheres*,
672 113, 10.1029/2008JD009944, 2008.

673 Ichikawa, H., and Yasunari, T.: Time-Space Characteristics of Diurnal Rainfall
674 over Borneo and Surrounding Oceans as Observed by TRMM-PR, *Journal of Climate*,
675 19, 1238-1260, 10.1175/jcli3714.1, 2006.

676 Jeong, G. R., and Wang, C.: Climate effects of seasonally varying Biomass Burning
677 emitted Carbonaceous Aerosols (BBCA), *Atmos. Chem. Phys.*, 10, 8373-8389,
678 10.5194/acp-10-8373-2010, 2010.

679 Jiang, J. H., Su, H., Huang, L., Wang, Y., Massie, S., Zhao, B., Omar, A., and Wang, Z.:
680 Contrasting effects on deep convective clouds by different types of aerosols, *Nature*
681 *Communications*, 9, 3874, 10.1038/s41467-018-06280-4, 2018.

682 Koh, T.-Y., and Teo, C.-K.: TOWARD A MESOSCALE OBSERVATION NETWORK IN
683 SOUTHEAST ASIA, *Bulletin of the American Meteorological Society*, 90, 481-488,
684 10.1175/2008bams2561.1, 2009.

685 Kunii, O., Kanagawa, S., Yajima, I., Hisamatsu, Y., Yamamura, S., Amagai, T., and
686 Ismail, I. T. S.: The 1997 Haze Disaster in Indonesia: Its Air Quality and Health
687 Effects, *Archives of Environmental Health: An International Journal*, 57, 16-22,
688 10.1080/00039890209602912, 2002.

689 Kurokawa, J., Ohara, T., Morikawa, T., Hanayama, S., Janssens-Maenhout, G.,
690 Fukui, T., Kawashima, K., and Akimoto, H.: Emissions of air pollutants and
691 greenhouse gases over Asian regions during 2000–2008: Regional Emission
692 inventory in ASia (REAS) version 2, *Atmos. Chem. Phys.*, 13, 11019-11058,
693 10.5194/acp-13-11019-2013, 2013.

694 Lee, H.-H., Bar-Or, R. Z., and Wang, C.: Biomass burning aerosols and the low-
695 visibility events in Southeast Asia, *Atmos. Chem. Phys.*, 17, 965-980, 10.5194/acp-
696 17-965-2017, 2017.

697 Lee, H.-H., Iraqi, O., Gu, Y., Yim, S. H. L., Chulakadabba, A., Tonks, A. Y. M., Yang,
698 Z., and Wang, C.: Impacts of air pollutants from fire and non-fire emissions on the
699 regional air quality in Southeast Asia, *Atmos. Chem. Phys.*, 18, 6141-6156,
700 10.5194/acp-18-6141-2018, 2018.

701 Lee, H.-H., Iraqi, O., and Wang, C.: The Impact of Future Fuel Consumption on
702 Regional Air Quality in Southeast Asia, *Scientific Reports*, 9, 2648, 10.1038/s41598-
703 019-39131-3, 2019.

704 Lin, J. C., Matsui, T., Pielke Sr., R. A., and Kummerow, C.: Effects of biomass-
705 burning-derived aerosols on precipitation and clouds in the Amazon Basin: a
706 satellite-based empirical study, *Journal of Geophysical Research: Atmospheres*, 111,
707 10.1029/2005jd006884, 2006.

708 Lin, N.-H., Tsay, S.-C., Maring, H. B., Yen, M.-C., Sheu, G.-R., Wang, S.-H., Chi, K. H.,
709 Chuang, M.-T., Ou-Yang, C.-F., Fu, J. S., Reid, J. S., Lee, C.-T., Wang, L.-C., Wang, J.-L.,
710 Hsu, C. N., Sayer, A. M., Holben, B. N., Chu, Y.-C., Nguyen, X. A., Sopajaree, K., Chen, S.-
711 J., Cheng, M.-T., Tsuang, B.-J., Tsai, C.-J., Peng, C.-M., Schnell, R. C., Conway, T., Chang,
712 C.-T., Lin, K.-S., Tsai, Y. I., Lee, W.-J., Chang, S.-C., Liu, J.-J., Chiang, W.-L., Huang, S.-J.,
713 Lin, T.-H., and Liu, G.-R.: An overview of regional experiments on biomass burning
714 aerosols and related pollutants in Southeast Asia: From BASE-ASIA and the Dongsha
715 Experiment to 7-SEAS, *Atmospheric Environment*, 78, 1-19,
716 <http://dx.doi.org/10.1016/j.atmosenv.2013.04.066>, 2013.

717 Lo, J. C. F., and Orton, T.: The general features of tropical Sumatra Squalls,
718 *Weather*, 71, 175-178, 10.1002/wea.2748, 2016.

719 Miettinen, J., Shi, C., and Liew, S. C.: Deforestation rates in insular Southeast Asia
720 between 2000 and 2010, *Global Change Biology*, 17, 2261-2270, 10.1111/j.1365-
721 2486.2011.02398.x, 2011.

722 Mlawer, E. J., Taubman, S. J., Brown, P. D., Iacono, M. J., and Clough, S. A.:
723 Radiative transfer for inhomogeneous atmospheres: RRTM, a validated correlated-k
724 model for the longwave, *Journal of Geophysical Research: Atmospheres*, 102, 16663-
725 16682, 10.1029/97JD00237, 1997.

726 Morrison, H., Curry, J. A., and Khvorostyanov, V. I.: A New Double-Moment
727 Microphysics Parameterization for Application in Cloud and Climate Models. Part I:
728 Description, *Journal of the Atmospheric Sciences*, 62, 1665-1677,
729 10.1175/jas3446.1, 2005.

730 Morrison, H., Thompson, G., and Tatarskii, V.: Impact of Cloud Microphysics on
731 the Development of Trailing Stratiform Precipitation in a Simulated Squall Line:
732 Comparison of One- and Two-Moment Schemes, *Monthly Weather Review*, 137,
733 991-1007, 10.1175/2008mwr2556.1, 2009.

734 Nakanishi, M., and Niino, H.: Development of an Improved Turbulence Closure
735 Model for the Atmospheric Boundary Layer, *Journal of the Meteorological Society of
736 Japan. Ser. II*, 87, 895-912, 10.2151/jmsj.87.895, 2009.

737 National Centers for Environmental Prediction, N. W. S. N. U. S. D. o. C.: NCEP FNL
738 Operational Model Global Tropospheric Analyses, continuing from July 1999,
739 10.5065/D6M043C6, 2000.

740 Oki, T., and Musiaka, K.: Seasonal Change of the Diurnal Cycle of Precipitation
741 over Japan and Malaysia, *Journal of Applied Meteorology*, 33, 1445-1463,
742 10.1175/1520-0450(1994)033<1445:scotdc>2.0.co;2, 1994.

743 Ramanathan, V., Crutzen, P. J., Lelieveld, J., Mitra, A. P., Althausen, D., Anderson, J.,
744 Andreae, M. O., Cantrell, W., Cass, G. R., Chung, C. E., Clarke, A. D., Coakley, J. A.,
745 Collins, W. D., Conant, W. C., Dulac, F., Heintzenberg, J., Heymsfield, A. J., Holben, B.,
746 Howell, S., Hudson, J., Jayaraman, A., Kiehl, J. T., Krishnamurti, T. N., Lubin, D.,
747 McFarquhar, G., Novakov, T., Ogren, J. A., Podgorny, I. A., Prather, K., Priestley, K.,
748 Prospero, J. M., Quinn, P. K., Rajeev, K., Rasch, P., Rupert, S., Sadourny, R., Satheesh, S.
749 K., Shaw, G. E., Sheridan, P., and Valero, F. P. J.: Indian Ocean Experiment: An

750 integrated analysis of the climate forcing and effects of the great Indo-Asian haze,
751 Journal of Geophysical Research: Atmospheres, 106, 28371-28398,
752 10.1029/2001jd900133, 2001.

753 Ramanathan, V., and Carmichael, G.: Global and regional climate changes due to
754 black carbon, Nature Geosci, 1, 221-227, 2008.

755 Rosenfeld, D.: TRMM observed first direct evidence of smoke from forest fires
756 inhibiting rainfall, Geophysical Research Letters, 26, 3105-3108,
757 10.1029/1999gl006066, 1999.

758 Rosenfeld, D., Lohmann, U., Raga, G. B., O'Dowd, C. D., Kulmala, M., Fuzzi, S.,
759 Reissell, A., and Andreae, M. O.: Flood or Drought: How Do Aerosols Affect
760 Precipitation?, Science, 321, 1309-1313, 10.1126/science.1160606, 2008.

761 Satheesh, S. K., and Ramanathan, V.: Large differences in tropical aerosol forcing
762 at the top of the atmosphere and Earth's surface, Nature, 405, 60-63,
763 10.1038/35011039, 2000.

764 Schell, B., Ackermann, I. J., Hass, H., Binkowski, F. S., and Ebel, A.: Modeling the
765 formation of secondary organic aerosol within a comprehensive air quality model
766 system, Journal of Geophysical Research: Atmospheres (1984–2012), 106, 28275-
767 28293, 2001.

768 Sekiguchi, M., Nakajima, T., Suzuki, K., Kawamoto, K., Higurashi, A., Rosenfeld, D.,
769 Sano, I., and Mukai, S.: A study of the direct and indirect effects of aerosols using
770 global satellite data sets of aerosol and cloud parameters, Journal of Geophysical
771 Research: Atmospheres, 108, 4699, 10.1029/2002JD003359, 2003.

772 Shi, H., Jiang, Z., Zhao, B., Li, Z., Chen, Y., Gu, Y., Jiang, J. H., Lee, M., Liou, K.-N., Neu,
773 J. L., Payne, V. H., Su, H., Wang, Y., Witek, M., and Worden, J.: Modeling Study of the
774 Air Quality Impact of Record-Breaking Southern California Wildfires in December
775 2017, Journal of Geophysical Research: Atmospheres, 124, 6554-6570,
776 10.1029/2019jd030472, 2019.

777 Stockwell, W. R., Kirchner, F., Kuhn, M., and Seefeld, S.: A new mechanism for
778 regional atmospheric chemistry modeling, Journal of Geophysical Research:
779 Atmospheres, 102, 25847-25879, 10.1029/97JD00849, 1997.

780 Taylor, D.: Biomass burning, humans and climate change in Southeast Asia,
781 Biodivers Conserv, 19, 1025-1042, 10.1007/s10531-009-9756-6, 2010.

782 Tewari, M., F. Chen, W. Wang, J. Dudhia, M. A. LeMone, K. Mitchell, M. Ek, G.
783 Gayno, J. Wegiel, and Cuenca, R. H.: Implementation and verification of the unified
784 NOAA land surface model in the WRF model, 20th conference on weather analysis
785 and forecasting/16th conference on numerical weather prediction, Seattle, WA,
786 U.S.A., 2004.

787 Tosca, M. G., Randerson, J. T., and Zender, C. S.: Global impact of smoke aerosols
788 from landscape fires on climate and the Hadley circulation, Atmos. Chem. Phys., 13,
789 5227-5241, 10.5194/acp-13-5227-2013, 2013.

790 Wagner, A., Heinzeller, D., Wagner, S., Rummler, T., and Kunstmann, H.: Explicit
791 Convection and Scale-Aware Cumulus Parameterizations: High-Resolution
792 Simulations over Areas of Different Topography in Germany, Monthly Weather
793 Review, 146, 1925-1944, 10.1175/mwr-d-17-0238.1, 2018.

794 Wang, C.: A modeling study on the climate impacts of black carbon aerosols,
795 Journal of Geophysical Research: Atmospheres, 109, n/a-n/a,
796 10.1029/2003JD004084, 2004.

797 Wang, C.: A modeling study of the response of tropical deep convection to the
798 increase of cloud condensation nuclei concentration: 1. Dynamics and microphysics,
799 Journal of Geophysical Research: Atmospheres, 110, D21211,
800 10.1029/2004JD005720, 2005.

801 Wiedinmyer, C., Akagi, S. K., Yokelson, R. J., Emmons, L. K., Al-Saadi, J. A., Orlando,
802 J. J., and Soja, A. J.: The Fire INventory from NCAR (FINN): a high resolution global
803 model to estimate the emissions from open burning, Geosci. Model Dev., 4, 625-641,
804 10.5194/gmd-4-625-2011, 2011.

805 Wu, P., Hara, M., Hamada, J.-i., Yamanaka, M. D., and Kimura, F.: Why a Large
806 Amount of Rain Falls over the Sea in the Vicinity of Western Sumatra Island during
807 Nighttime, Journal of Applied Meteorology and Climatology, 48, 1345-1361,
808 10.1175/2009jamc2052.1, 2009.

809 Wu, R., Wen, Z., and He, Z.: ENSO Contribution to Aerosol Variations over the
810 Maritime Continent and the Western North Pacific during 2000–10, Journal of
811 Climate, 26, 6541-6560, 10.1175/JCLI-D-12-00253.1, 2013.

812 Yi, L., and Lim, H.: Semi-Idealized COAMPS® Simulations of Sumatra Squall
813 Lines: the Role of Boundary Forcing, in: Advances in Geosciences, 111-124, 2006.

814 Zhang, Y., Fan, J., Logan, T., Li, Z., and Homeyer, C. R.: Wildfire impact on
815 environmental thermodynamics and severe convective storms, Geophysical
816 Research Letters, 0, 10.1029/2019gl084534, 2019.

817 Zhao, B., Gu, Y., Liou, K.-N., Wang, Y., Liu, X., Huang, L., Jiang, J. H., and Su, H.:
818 Type-Dependent Responses of Ice Cloud Properties to Aerosols From Satellite
819 Retrievals, Geophysical Research Letters, 45, 3297-3306, 10.1002/2018gl077261,
820 2018.

821

822

823
824

Table 1. The case period of the selected cases in the Sumatra region (r1) and the Borneo region (r2)

Case name	Case period
r1c1	2008/08/10 0900 UTC ~ 2008/08/11 0300 UTC
r1c2	2008/08/19 0600 UTC ~ 2008/08/20 0000 UTC
r1c3	2008/09/23 0900 UTC ~ 2008/09/24 0000 UTC
r2c1	2008/08/05 0900 UTC ~ 2008/08/06 0300 UTC
r2c2	2008/09/17 0600 UTC ~ 2008/09/17 2100 UTC
r2c3	2008/09/22 0300 UTC ~ 2008/09/23 0000 UTC

825
826
827

828

Table 2. The fire periods in the two study regions

The Sumatra region (r1)	The Borneo region (r2)
6/10/2008 ~ 6/20/2008	6/21/2008 ~ 6/27/2008
6/25/2008 ~ 6/28/2008	8/1/2008 ~ 8/8/2008
7/4/2008 ~ 7/7/2008	9/10/2008 ~ 9/30/2008
7/27/2008 ~ 8/20/2008	
9/17/2008 ~ 9/27/2008	

829

830

831 Table 3. The mean differences in percentage of FFBB to FF (i.e. $(FFBB-FF)/FF \times 100\%$)
 832 for each selected case over the main convection area in the Sumatra region (r1) and the
 833 Borneo region (r2). Qc, Qi, Qr, Qs and Qg represents cloud, ice, rain, snow, and graupel
 834 mass concentration respectively. Qnc, Qni, Qnr, Qns and Qng means number
 835 concentration for each hydrometeor.

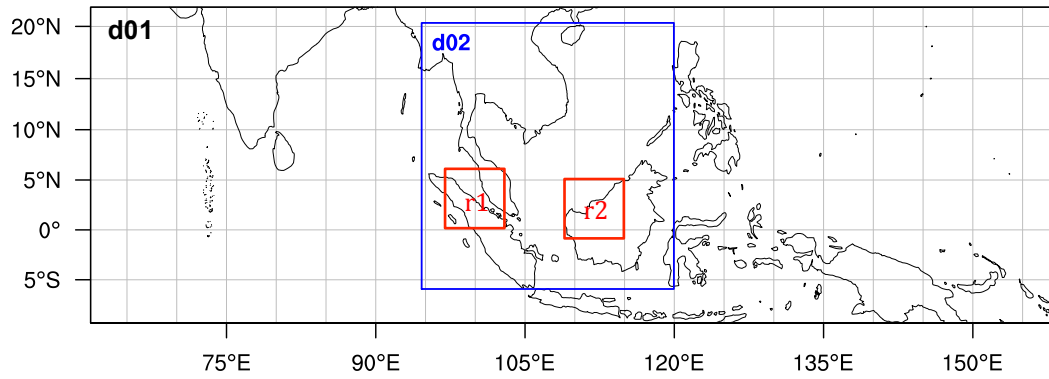
Case	Qc	Qi	Qr	Qs	Qg	Qnc	Qni	Qnr	Qns	Qng
r1c1	8%	27%	49%	62%	48%	248%	55%	-41%	33%	39%
r1c2	20%	-6%	-15%	-25%	1%	349%	-1%	-45%	-11%	-6%
r1c3	18%	10%	-10%	3%	5%	311%	4%	-50%	11%	-6%
r2c1	27%	1%	-6%	-5%	-4%	703%	3%	-59%	4%	-5%
r2c2	22%	10%	64%	69%	58%	337%	24%	-32%	17%	57%
r3c3	8%	10%	19%	60%	-2%	409%	-5%	-66%	8%	-12%

836

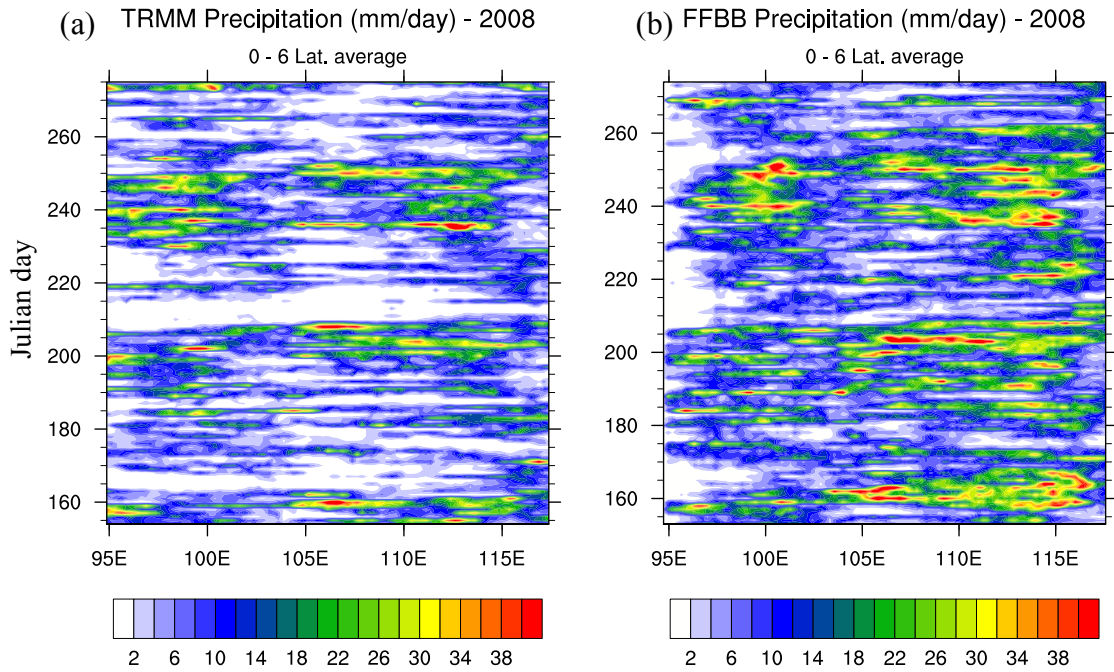
837 Table 4. The averaged precipitation ($\text{mm } 3\text{hrs}^{-1}$) of FFBB and FF for each selected case
 838 over the main convection area in the Sumatra region (r1) and the Borneo region (r2).
 839 Parentheses in the third column show the difference in percentage of FFBB to FF (i.e.
 840 $(\text{FFBB}-\text{FF})/\text{FF} \times 100\%$).
 841

Case	FF	FFBB
r1c1	1.33±0.47	2.74±1.21 (+106%)
r1c2	2.97±1.42	3.05±1.49 (+3%)
r1c3	4.32±1.84	3.98±2.18 (-8%)
r2c1	3.73±2.64	3.07±1.21 (-18%)
r2c2	1.88±0.53	3.97±1.47 (+111%)
r3c3	0.54±0.53	1.10±1.02 (+103%)

842
 843



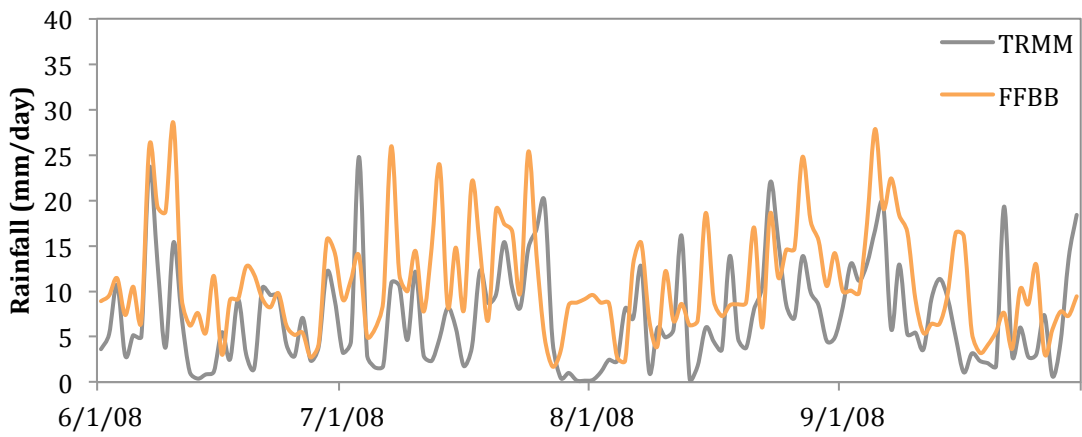
844
845 Figure 1. Domain configuration for WRF-Chem simulations. Domain 1 (d01) has a
846 resolution of 25 km, while Domain 2 (d02) has a resolution of 5 km. Two red boxes
847 indicate the two study regions: the Sumatra region (r1) and the Borneo region (r2).
848
849
850



851
852
853
854
855

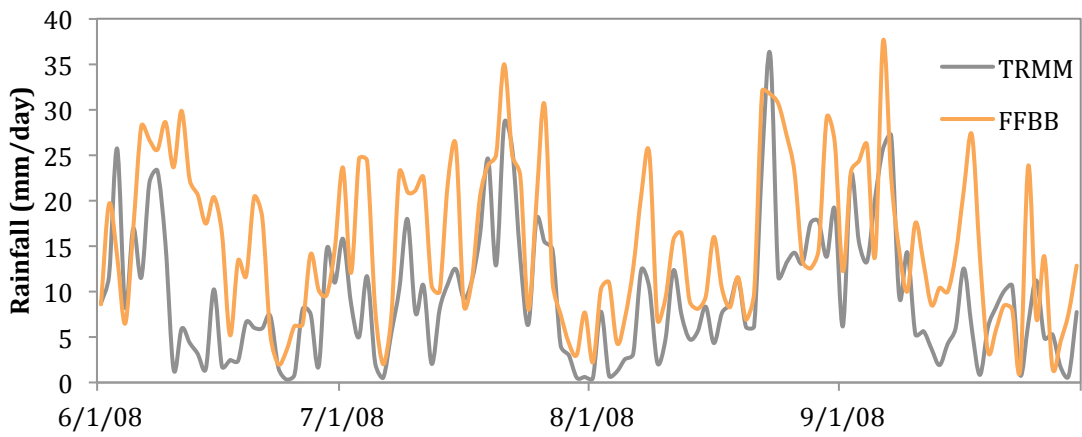
Figure 2. Hovmöller (time versus longitude) plot of daily precipitation (mm day^{-1}) from 1 June 2008 to 30 September 2008 from:(a) Tropical Rainfall Measuring Mission (TRMM) and (b) FFBB. Latitude average is from 0° to 6°N .

(a) Rainfall comparison - r1



856

(b) Rainfall comparison - r2



857

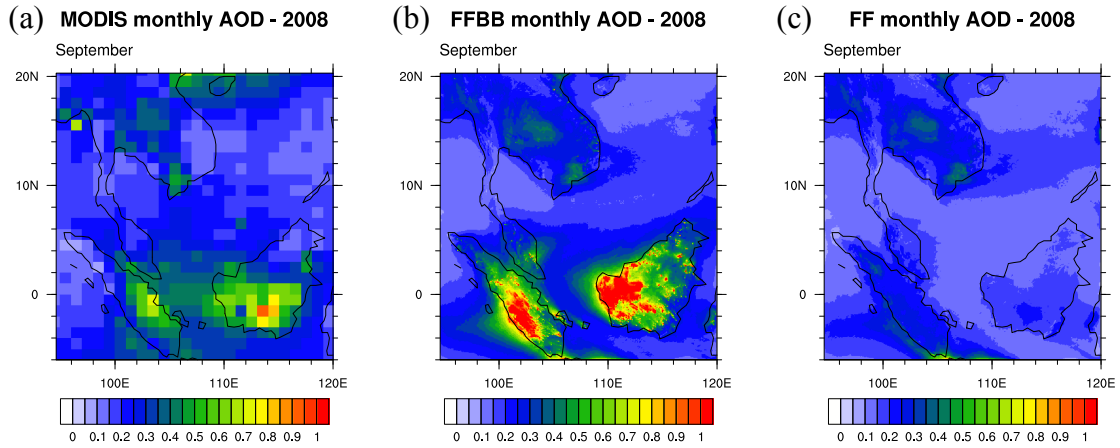
858

859

860

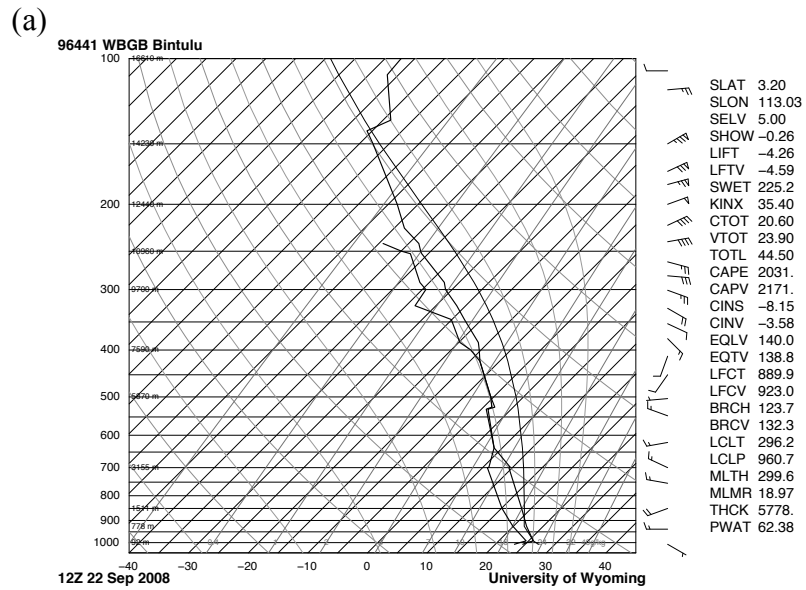
861

Figure 3. Time series of area-averaged daily rainfall (mm day^{-1}) from Tropical Rainfall Measuring Mission (TRMM) and FFBB over (a) the Sumatra region (r1) and (b) the Borneo region (r2).

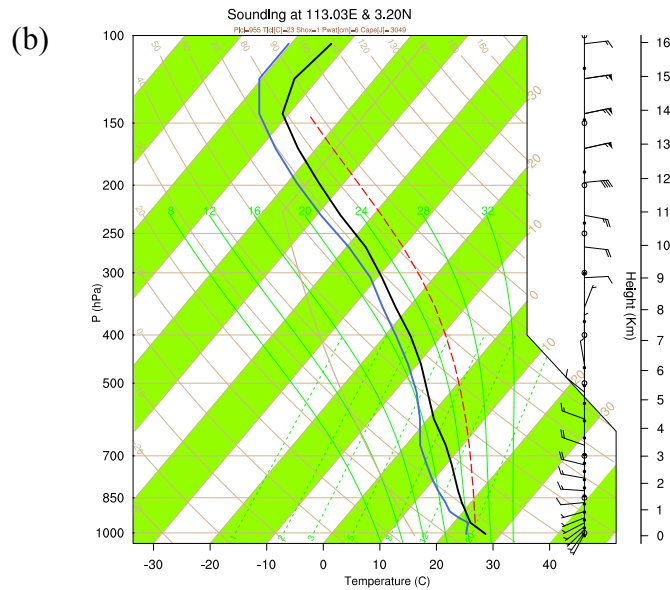


862
 863
 864
 865
 866

Figure 4. Monthly aerosol optical depth (AOD) in September 2008 from (a) Moderate Resolution Imaging Spectroradiometer (MODIS), (b) FFBB, and (c) FF.



867



868

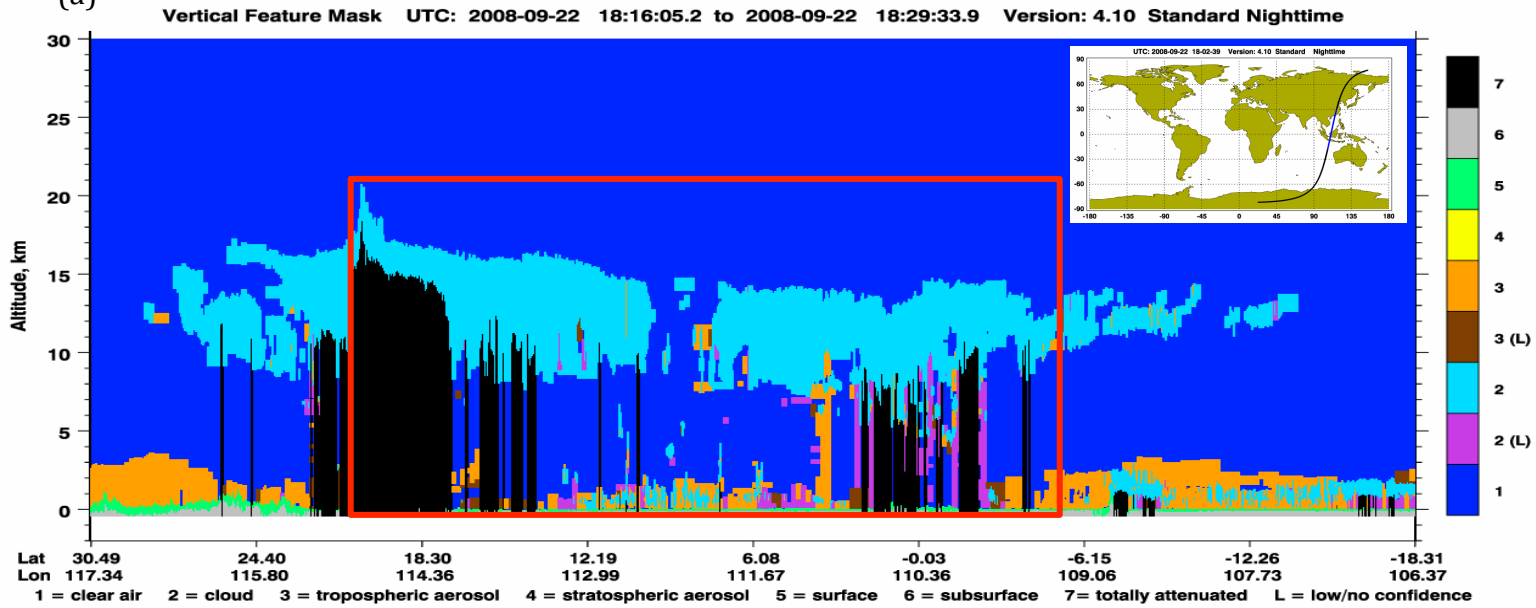
869

870

871

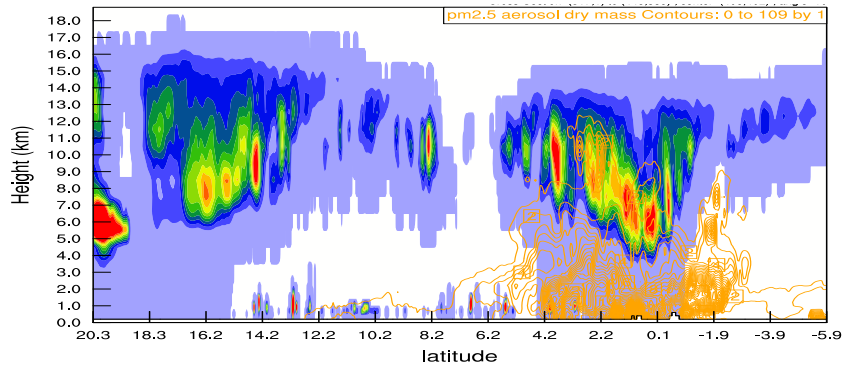
Figure 5. (a) Sounding profile observed at Bintulu Airport, Malaysia (113.03° E, 3.20° N) at 12 UTC on 22 September 2008. (b) Modeled sounding profile in FFBB at the same location and time as (a).

(a)

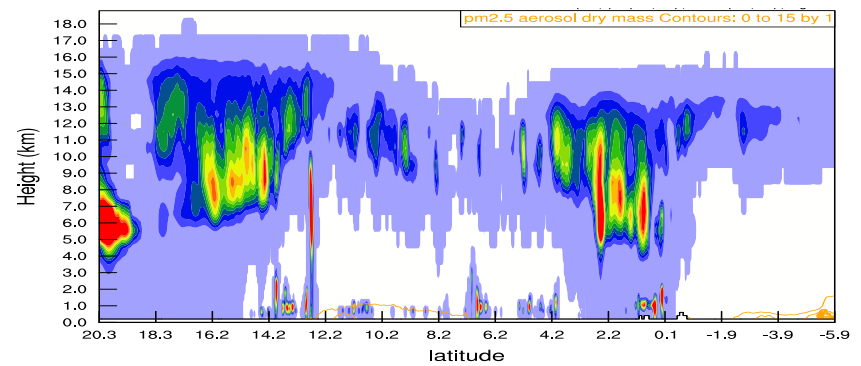


872
873
874

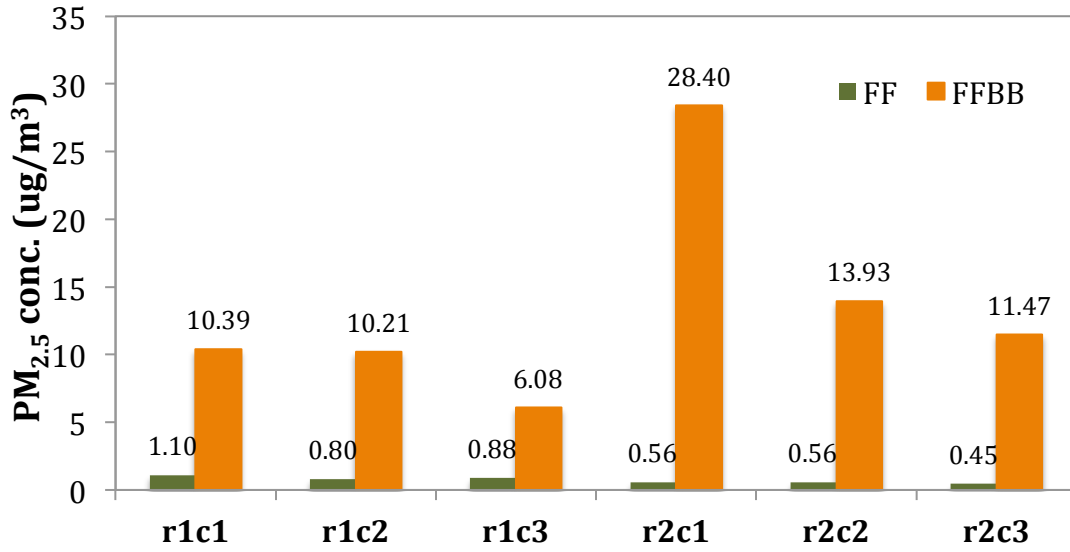
(b)



(c)



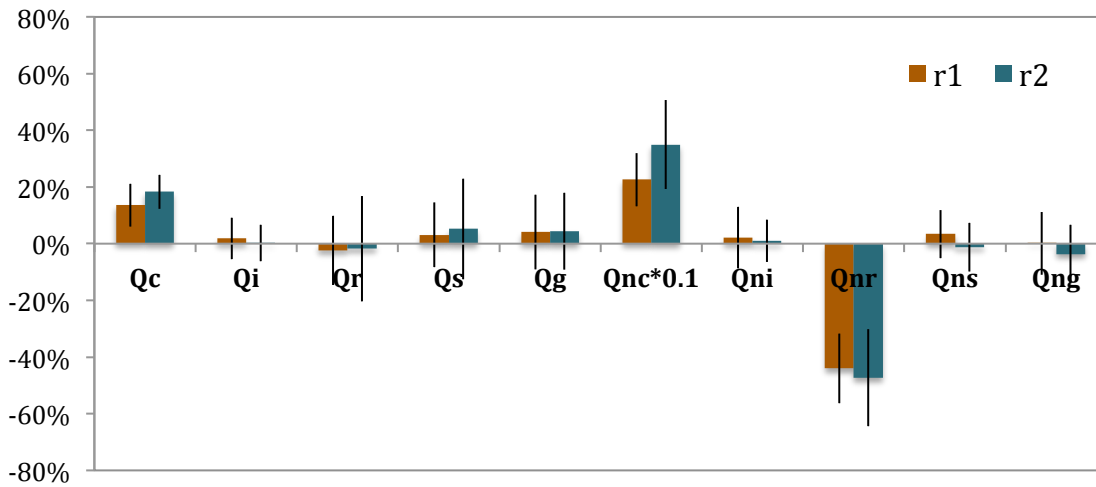
876 Figure 6 (a) The vertical structure of cloud retrieved from the Cloud-Aerosol Lidar and Infrared Pathfinder Satellite Observation
877 (CALIPSO) on September 22, 2008. (b)-(c) The sum of simulated hydrometeor mixing ratio (shaded; kg kg^{-1}) and $\text{PM}_{2.5}$ concentration
878 (contour; $\mu\text{g m}^{-3}$) in FFBB and FF, respectively. The profile domain of (b) and (c) is corresponding to the red rectangle in (a).
879



867
868
869
870

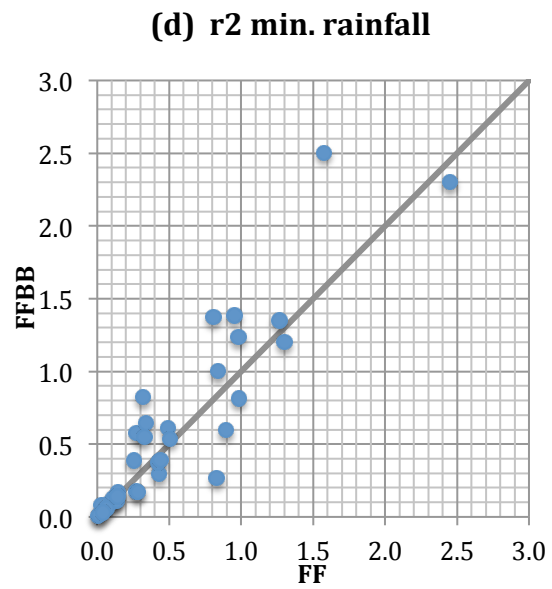
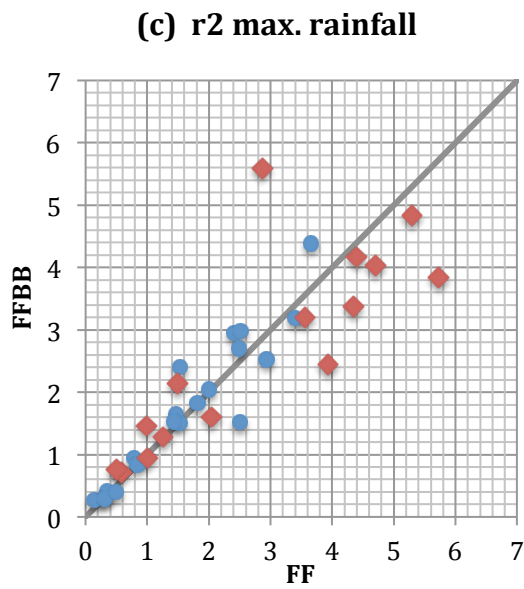
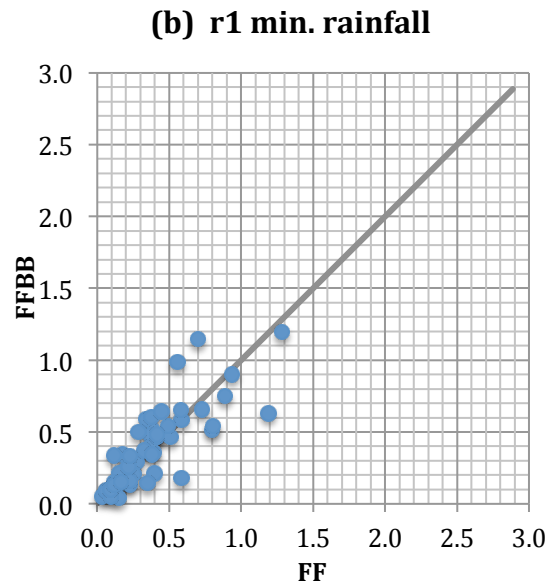
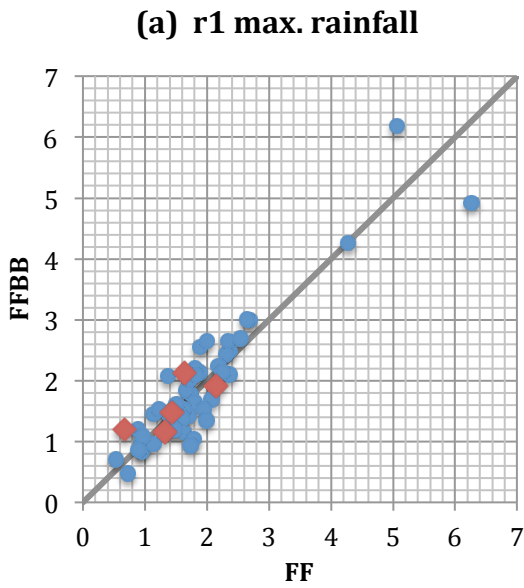
Figure 7. The mean PM_{2.5} concentration ($\mu\text{g m}^{-3}$) in FF and FFBB for selected cases in the Sumatra region (r1) and the Borneo region (r2).

884
885



886
887
888
889
890
891
892
893

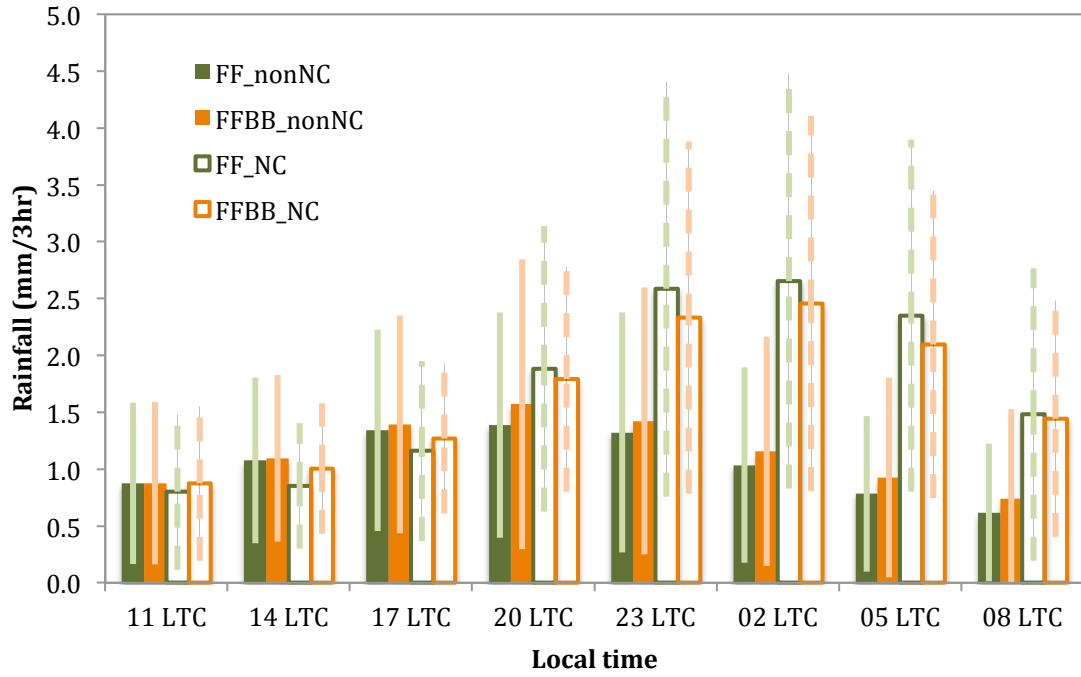
Figure 8. The mean differences in percentage of FFBB to FF (i.e. $(FFBB-FF)/FF \times 100\%$) over all convective cases during the fire periods in the Sumatra region (r1) and the Borneo region (r2). Qc, Qi, Qr, Qs and Qg represents cloud, ice, rain, snow, and graupel mass concentration, respectively. Qnc, Qni, Qnr, Qns and Qng means number concentration for each hydrometeor. The error bars represent one standard deviation.



894

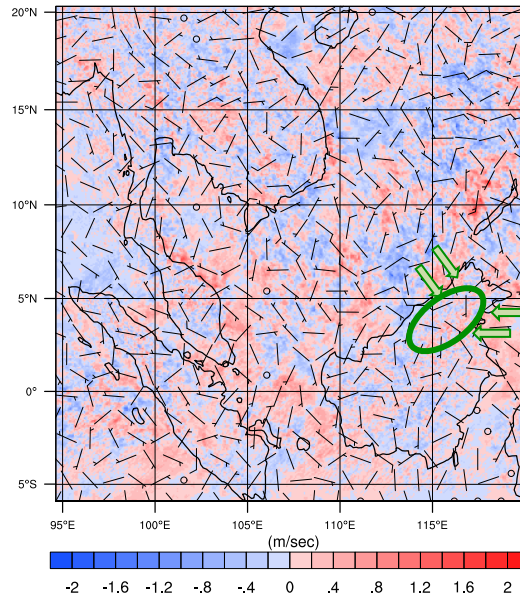
895
896
897
898
899
900
901

Figure 9. The scatterplots of daily maximum and minimum convective rainfall ($\text{mm } 3\text{hr}^{-1}$) during the fire periods in in the Sumatra region (r1) and the Borneo region (r2). Red diamonds in (a) and (c) indicate that the maximum convective rainfall conducts in the midnight or early morning.



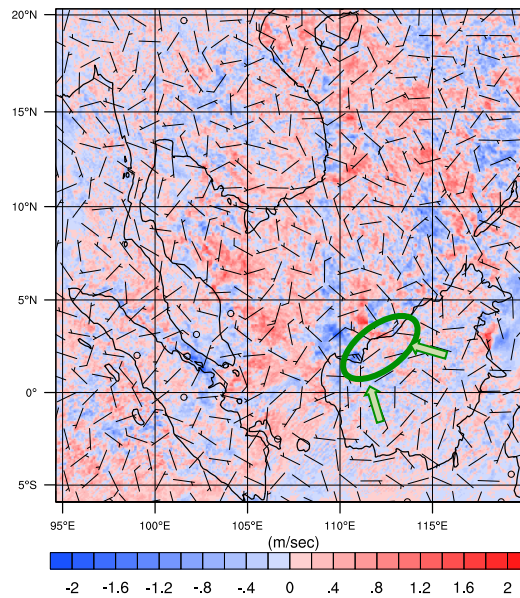
902
 903 Figure 10. The diurnal time series of rainfall averaged over the Borneo region (r2) for
 904 nocturnal convections (NC) and non- nocturnal convections (non-NC) during fire periods in
 905 FF and FFBB. The error bars denote the standard deviation of the rainfall.
 906
 907

(a)



908

(b)



909

910

911

912

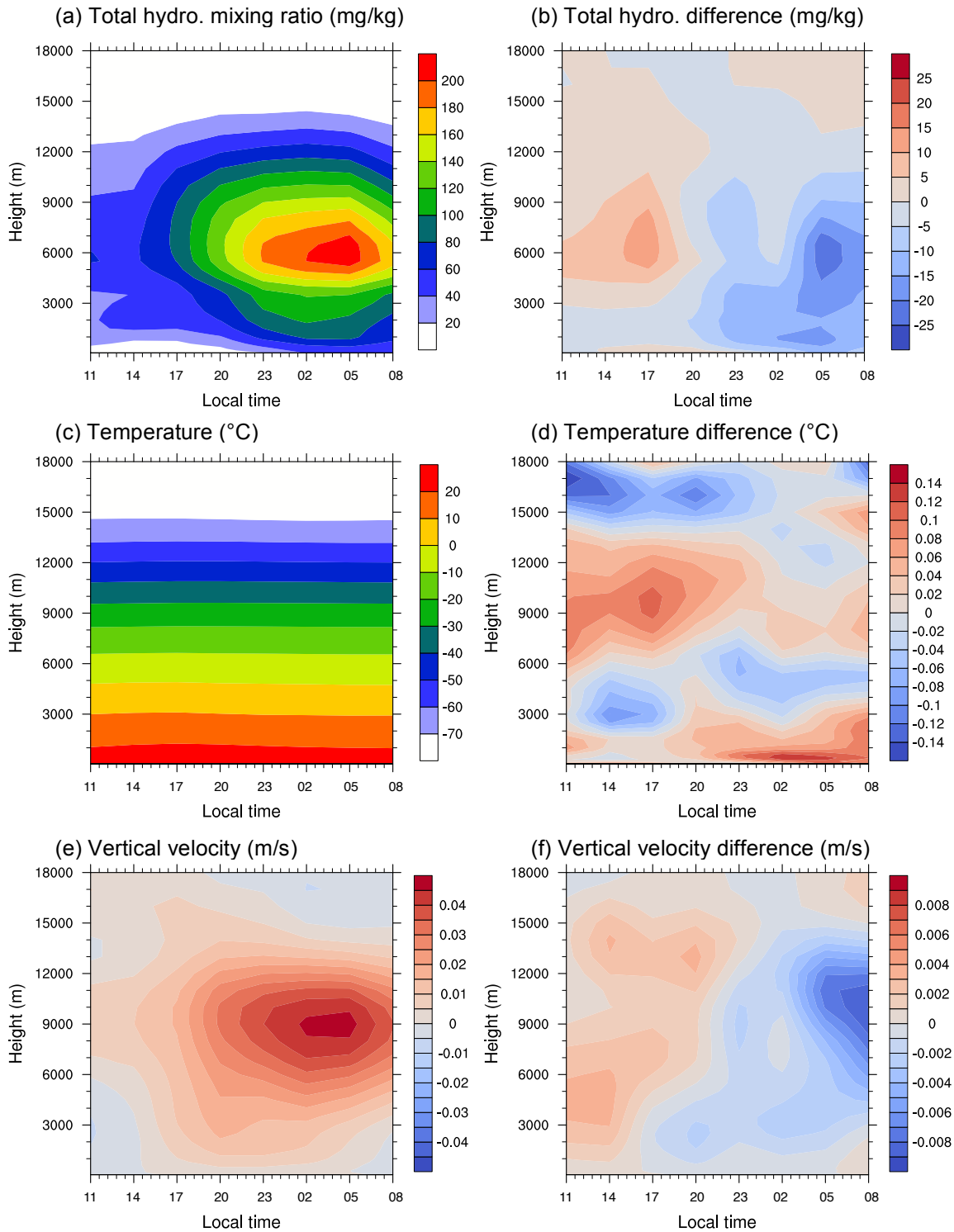
913

914

915

916

Figure 11. The mean wind field differences of FFBB and FF (FFBB-FF) at (a) 20 LST for non-nocturnal cases and (b) 02 LST for nocturnal cases in the Borneo region (r2). The green circle indicates the location of convections occurred. The green arrows mean the mean flow of sea breeze in (a) and land breeze in (b). The magnitude of wind barbs is 10 times higher than the real value.



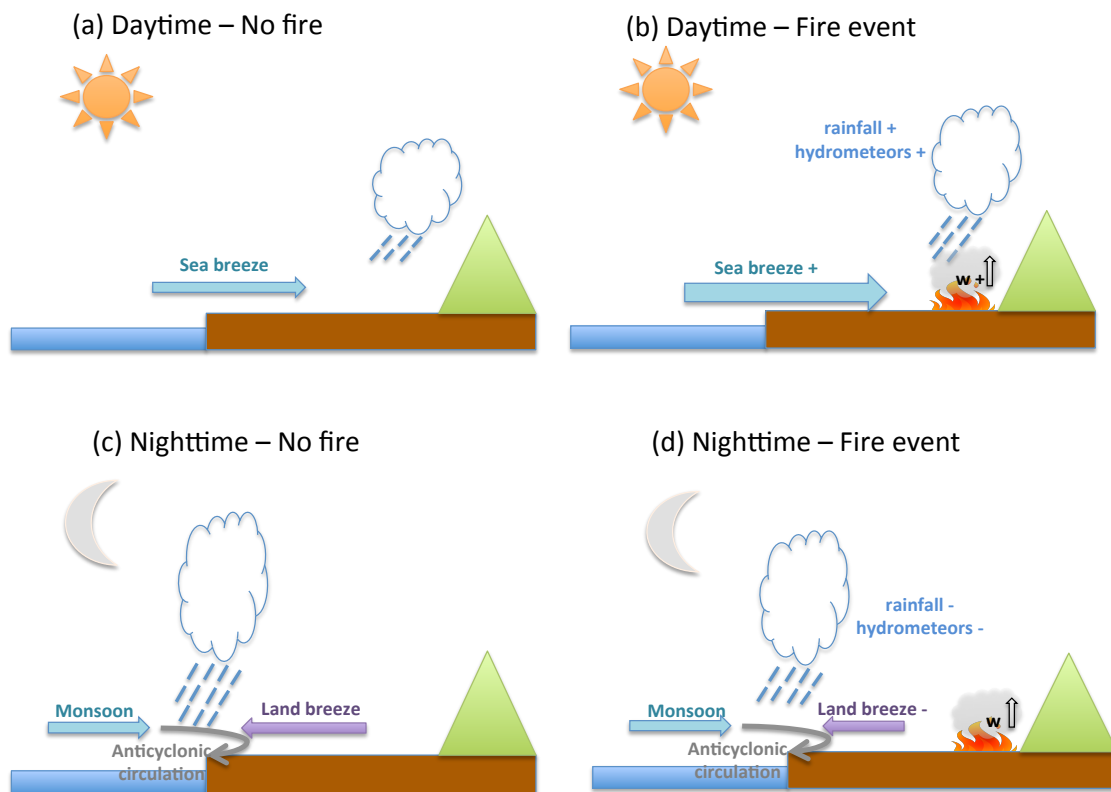
917
918

919
920

921

922 Figure 12. Diurnal evolution of vertical profiles over the Borneo region (r2) in FF for (a)
923 total hydrometeor mixing ratio (mg kg^{-1}), (c) temperature ($^{\circ}\text{C}$), and (e) vertical velocity (m s^{-1}).
924 Data are averaged all the nocturnal convections. (b), (d), and (f) is the differences
925 between FF and FFBB (FFBB-FF) for each parameter.

926



928
 929
 930
 931
 932

Figure 13. Schematics of diurnal rainfall/convection activity over the western Borneo. (a) and (b) illustrate the formation of convection during the daytime without and with fire event, respectively. (c) and (d) are the same as (a) and (b) but in the nighttime.